Inhibition of *Mycobacterium tuberculosis* DosRST two-component regulatory system signaling by targeting response regulator DNA binding and sensor kinase heme

Huiqing Zheng[1], Bilal Aleiwi[2], Edmund Ellsworth[2], and Robert B. Abramovitch[1*]

[1]Department of Microbiology and Molecular Genetics, [2]Department of Pharmacology and Toxicology, Michigan State University, East Lansing, Michigan, 48824

[*]*Corresponding Author*

Robert B. Abramovitch

E-mail: abramov5@msu.edu

Phone: (517) 884-5416

Fax: (517) 353-8957

Abstract

Mycobacterium tuberculosis (Mtb) possesses a two-component regulatory system, DosRST, that enables Mtb to sense host immune cues and establish a state of non-replicating persistence (NRP). NRP bacteria are tolerant to several anti-mycobacterial drugs and are thought to play a role in the long course of tuberculosis (TB) therapy. Therefore, small molecules that inhibit Mtb from establishing or maintaining NRP could reduce the reservoir of drug tolerant bacteria and function as an adjunct therapy to reduce treatment time. Previously, we reported the discovery of six novel chemical inhibitors of DosRST, named HC101A-106A, from a whole cell, reporter-based phenotypic high throughput screen. Here, we report functional and mechanism of action studies of HC104A and HC106A. RNAseq transcriptional profiling shows that the compounds downregulate genes of the DosRST regulon. Both compounds reduce hypoxia-induced triacylglycerol synthesis by ~50%. HC106A inhibits Mtb survival during hypoxia-induced NRP, however, HC104A did not inhibit survival during NRP. An electrophoretic mobility assay shows that HC104A inhibits DosR DNA binding in a dose-dependent manner, indicating that HC104A may function by directly targeting DosR. In contrast, UV-visible spectroscopy studies suggest HC106A directly targets the histidine kinase heme, via a mechanism that is distinct from the oxidation and alkylation of heme previously observed with artemisinin (HC101A). Synergistic interactions were observed when DosRST inhibitors were examined in pair-wise combinations with the strongest potentiation observed between artemisinin paired with HC102A, HC103A, or HC106A. Our data collectively show that the DosRST pathway can be inhibited by multiple distinct mechanisms.

Keywords: Chemical biology, two-component regulatory systems, microbial pathogenesis.

50 **Introduction**

51 *Mycobacterium tuberculosis* (Mtb) is the causative agent of tuberculosis (TB). Mtb is an
52 intracellular pathogen that can latently infect the host without causing disease symptoms (1).
53 During chronic infection, it can establish a dormant state known as non-replicating persistence
54 (NRP) where Mtb modulates its metabolism in response to environmental and host immune
55 cues, such as hypoxia, acidic pH, and nutrient starvation (2, 3). DosRST is a two-component
56 regulatory system that regulates Mtb persistence (4-6). It consists of two sensor histidine
57 kinases, DosS and DosT, and the cognate response regulator DosR, which regulates
58 expression of about 50 genes in the DosRST regulon (6-8). The pathway can be induced by
59 host intracellular stimuli, such as nitric oxide (NO), carbon monoxide (CO) and hypoxia, through
60 DosS and DosT (9-11). DosS is an oxygen and redox sensor, whereas DosT acts an oxygen
61 sensor (12-14). Both kinases sense ligands via the heme group, and are inactive when the
62 heme exists as either the Met (Fe^{3+}) form (DosS) or the oxy (Fe^{2+}-O_2) form (DosT) in the
63 presence of O_2 (13). However, hypoxic conditions activate the kinases by inducing the
64 conversion of DosS to the ferrous form and DosT to the deoxy form. Therefore, DosS/T play
65 overlapping and distinct roles in sensing the redox status and oxygen level of the environment
66 to turn on the DosR pathway (11, 15).

67 Non-replicating bacilli are naturally tolerant to many anti-mycobacterial drugs, such as
68 isoniazid (INH) that only kills replicating Mtb (16-18). During TB infection, the disease presents
69 as a spectrum of replicating and non-replicating bacteria; the NRP population of bacteria are
70 thought to be responsible, in part, for the 6-month long course of TB treatment. This long
71 antibiotic regimen makes controlling the TB epidemic challenging and has likely contributed to
72 the evolution of drug-resistant Mtb strains. Therefore, there exists an urgent need to identify
73 new strategies to treat the disease, with a particular focus on discovering new ways to shorten
74 the course of TB therapy. Targeting the DosRST pathway is a promising strategy, because
75 *dosRST* mutants are attenuated in *in vitro* models of hypoxia-driven NRP (19) and in animal

76 models that generate hypoxic granulomas, including non-human primates, guinea pigs, and
77 C3HeB/FeJ mouse models of TB infection (4, 20-22). Furthermore, deletion of DosR-regulated
78 gene *tgs1*, which is involved in triacylglycerol (TAG) synthesis, causes reduced antibiotic
79 tolerance (23, 24). Therefore, inhibiting the DosRST pathway and killing the reservoir of NRP
80 bacteria may function to narrow the spectrum of TB disease and shorten the course of TB
81 therapy.

82 Fluorescent reporter strains can be used as tools in drug discovery to conduct targeted,
83 whole cell phenotypic screens for pathways that play a role during pathogenesis, but have
84 limited impact when bacteria are grown *in vitro*(25, 26). In an effort to discover the new chemical
85 probes that inhibit Mtb persistence, we previously performed a whole cell phenotypic high
86 throughput screening (HTS) of a >540,000 compound library using the DosRST regulon reporter
87 strain CDC1551 (*hspX'::*GFP) (27). We discovered six compounds that inhibit the DosR-
88 dependent, hypoxia-induced GFP fluorescence. In the previous report, we showed that the
89 HC101, HC102 and HC103 series functioned to inhibit NRP associated physiologies, including
90 TAG accumulation, survival during hypoxia and isoniazid tolerance. Mechanism of action
91 studies showed that the HC101 series, composed of artemisinin and related analogs, functioned
92 by oxidizing and alkylating the DosS and DosT heme. HC102 and HC103 did not modulate the
93 DosS/T heme, and were instead found to inhibit sensor kinase autophosphorylation. Here, we
94 report the characterization of two additional compounds, HC104A and HC106A. Transcriptional
95 and biochemical analysis demonstrate that both compounds function to downregulate the
96 DosRST pathway and inhibit persistence associated physiologies. Biochemical studies show
97 HC104A and HC106A function by distinct mechanisms of action, with HC104A inhibiting DosR
98 DNA binding and HC106A interacting with DosS and DosT heme to block environmental
99 sensing. Studies examining the pair-wise interactions between the five DosRST inhibitors
100 revealed synergistic interactions, including strong potentiating interactions of artermisinin and
101 HC106A. Structure activity relationship studies of HC106 identified functional groups of HC106A

102 that are required for activity and enabled optimization of HC106 potency to nanomolar effective
103 concentrations against whole cell Mtb.
104
105 **Results**
106 ***Inhibition of the DosR regulon by HC104A and HC106A***
107 Characterization studies were undertaken with two putative DosRST regulon inhibitors,
108 HC104A and HC106A (Fig. 1a) (27). Half-maximal effective concentration (EC_{50}) studies using
109 the CDC1551 (*hspX'::GFP*) DosRST-dependent fluorescent reporter strain, show that HC104A
110 and HC106A inhibit DosRST-dependent GFP florescence with EC_{50} values of 9.8 μM and 2.48
111 μM, respectively (Fig. 1b and 1c).
112 The compounds have minimal impact on Mtb growth, suggesting they are also potential
113 DosRST inhibitors, as DosRST is not required for survival under the conditions of mild hypoxia
114 used in the reporter-based assay. RNA-seq-based transcriptional profiling was undertaken to
115 determine if the DosRST regulon was inhibited by the compounds. Mtb was treated with 40 μM
116 HC104A, HC106A or dimethyl sulfoxide (DMSO) control for 6 d in a standing flask, and following
117 incubation RNA was extracted, sequenced and analyzed for differential gene expression relative
118 to the DMSO control. As a control for the DosR regulon, transcriptional profiling was also
119 previously conducted on a DMSO treated CDC1551(Δ*dosR*) mutant strain (27). The
120 transcriptional profiles showed that the genes strongly repressed by HC104A and HC106A (>2-
121 fold; $q<0.05$) are from the *dosR* regulon (Fig. 2a-c, Supplementary Dataset 1, 3).
122 HC106A exhibited a remarkably strong reduction of gene expression, with transcripts for
123 *tgs1* and *hspX* being almost undetectable by RNA-seq following HC106A treatment.
124 Interestingly, while HC106A broadly inhibited genes of the DosRST regulon, HC104A only
125 strongly inhibited part of the DosR regulon, with the strongest inhibition reserved for *hspX*, the
126 promoter used to drive reporter fluorescence in the screen. These RNA-seq results were

127 validated by semi-quantitative RT-PCR, with HC104A causing downregulation of *dosR*, *hspX*,
128 and *tgs1 in vitro* by 6-, 570- and 13-fold, respectively; whereas HC106A downregulated these
129 three genes by 49-, 1360-, and 1424-fold, respectively (Supplementary Fig. 1), with *hspX* and
130 *tgs1* transcripts being below the level of detection by qRT-PCR.

131 Comparisons of transcriptional profiles from the inhibitor treated wild type (WT) Mtb
132 strain to a CDC1551(Δ*dosR*) mutant strain showed that there are a total of 26 genes and 53
133 genes from *dosR* regulon inhibited by HC104A and HC106A, respectively. Notably, HC104A
134 and HC106A caused an additional 119 genes and 35 genes to be repressed that were not
135 repressed in the CDC1551(Δ*dosR*) mutant strain (Fig. 2c). This observation suggested that
136 these two compounds exhibit some DosR-independent activities. To confirm the specificity of
137 the compounds, RNA-seq was also performed on CDC1551(Δ*dosR*) mutant background
138 (Supplementary Dataset 2-3) treated with HC104A or HC106A. This analysis identified 171
139 genes and 51 genes that are downregulated (>2-fold; $q<0.05$) by HC104A and HC106A,
140 respectively (Fig. 2d). This finding indicates that HC104A and HC106A impact other targets
141 beside DosR regulon, with HC106A showing greater on-target specificity than HC104A. Based
142 on these findings, we conclude that: 1) HC106A strongly and specifically inhibits the DosRST
143 regulon; and 2) HC104A strongly inhibits a portion of the DosRST regulon, with several notable
144 off-target activities.

145 To assess the impact of the inhibitors on the DosRST pathway on intracellular Mtb,
146 murine bone marrow-derived mouse macrophages were infected with Mtb and treated with 40
147 μM HC104A and HC106A for 48 h. Total bacterial RNA was isolated and analyzed by RT-PCR
148 for *hspX* and *tgs1* gene differential expression. The results demonstrate that the induction of
149 *hspX* and *tgs1* were inhibited 185- and 10-fold by HC104A and 6- and 4-fold by HC106A,
150 respectively (Fig. 3a). These finding confirm that HC104A and HC106A can access Mtb inside

151 the macrophage, however, the reduced repression of the pathway by HC106A as compared to
152 broth culture, suggests that the molecule may not be able to efficiently target intracellular Mtb.
153 The DosRST pathway is also induced by redox signals such as vitamin C and NO (27).
154 To examine whether HC104A and HC106A can repress the induction of DosRST pathway by
155 vitamin C or NO, Mtb cells were pretreated with HC104A or HC106A for 24 h followed by
156 vitamin C or NO induction for 2 h. The expression of DosR-regulated genes (*hspX* and *tgs1*)
157 was examined by real time-PCR. Vitamin C and DETA-NONOate (NO donor) strongly induced
158 *hspX* and *tgs1* as previously reported ((27), Fig. 3b). For instance, vitamin C induced *hspX* and
159 *tgs1* by 2162- and 58-fold, respectively; whereas DETA-NONOate upregulated *hspX* and *tgs1*
160 3024- and 113-fold, respectively (Fig. 3b). Mtb cells pretreated with HC106A showed strong
161 inhibition of *hspX* and *tgs1* induction by vitamin C and DETA-NONOate. For example, HC106A
162 inhibited the *hspX* and *tgs1* transcripts by 78- and 14-fold following vitamin C treatment,
163 respectively, and 362- and 151-fold following DETA-NONOate treatment. Following vitamin C
164 treatment, HC104 showed inhibition of *hspX* by 3.4-fold and no effect on *tgs1*, or 302- and 6.6-
165 fold inhibition of *hspX* and *tgs1* following DETA-NONOate treatment. These findings show that
166 HC104A and HC106A act as inhibitors of the DosRST pathway in response to redox signals in
167 addition to hypoxia.
168
169 ***Inhibition of Mtb persistence-associated physiologies***
170 Mtb accumulates TAG during hypoxia (27-29). DosR directly regulates *tgs1*, which
171 encodes a TAG synthase that is involved in the last step of TAG biosynthesis and is required for
172 TAG accumulation during hypoxia (30). Transcriptional profiling showed that HC104A and
173 HC106A repress expression of *tgs1*. Based on this transcriptional profiling, we hypothesized
174 these two compounds may inhibit TAG biosynthesis during NRP. To test our hypothesis, Mtb
175 cells were radiolabeled with ^{14}C-acetate and treated with HC104A or HC106A for 6 d. Lipids
176 were isolated and analyzed by thin layer chromatography (TLC). As previously observed,

177 DMSO treated CDC1551(Δ*dosR*) mutant displayed a strong (87%) reduction of TAG
178 accumulation as compared to DMSO treated WT (Fig. 3c and Supplementary Fig. 2). Mtb cells
179 treated with HC104A or HC106A showed a ~50% reduction of TAG accumulation, supporting
180 our hypothesis that the compounds can inhibit TAG biosynthesis.

181 DosRST has been previously reported to be required for survival during NRP, where
182 deletion of DosR causes greatly reduced survival during prolonged hypoxic stress (19). The
183 impact of HC104A and HC106A on Mtb survival during NRP was examined using the hypoxic
184 shift-down model (27). Mtb survival was examined following 10 d of treatment with the
185 compounds at 40 μM. The Δ*dosR* mutant control had 15% survival relative to DMSO, and was
186 partially complemented, supporting the proposal that survival during hypoxia is DosR
187 dependent. Mtb cells treated with HC106A displayed 50% survival relative to DMSO control
188 (Fig. 3d), whereas, HC104A had no impact on Mtb survival during NRP, an observation that
189 suggests the portion of the DosR regulon inhibited by HC104A is not essential for survival
190 during NRP.

191

192 ***HC104A inhibits DosR DNA binding***

193 There are several potential targets of HC104A and HC106A to directly inhibit DosRST
194 signaling, including: 1) direct inhibition of DosS/T sensor kinase activity, 2) modulation of the
195 heme in the sensor, or 3) inhibition of DosR binding of DNA. To investigate the biochemical
196 mechanisms of action of HC104A and HC106A, inhibition of DosS autophosphorylation was
197 initially evaluated. The DosS protein was treated with different concentrations of HC104A and
198 HC106A from 10 μM to 40 μM, or with 40 μM HC103A as a positive control that was previously
199 discovered to be a DosS/T autophosphorylation inhibitor (27). As previously observed, HC103A
200 strongly inhibited DosS autophosphorylation, but HC104A and HC106A had no inhibitory activity

201 (Supplementary Fig. 3). This suggests HC104A and HC106A are not directly inhibiting DosS/T
202 autophosphorylation activity.

203 Next, a UV-visible spectroscopy assay was employed to investigate if HC104A targets to
204 the heme of the sensor kinase DosS. Treatment of DosS protein with the reducing agent
205 dithionite (DTN) caused a shift of the Soret peak from 403 nm to 430 nm as previously
206 described (13, 27). Addition of HC104A to reduced DosS did not shift the peak to the oxidized
207 position, suggesting that HC104A does no modulate DosS heme redox (Supplementary Fig. 4).
208 Together, these data indicate that HC104A does not inhibit DosRST signaling by targeting
209 sensor kinase autophosphoryation or heme and supported examining DosR as a potential
210 target.

211 Inspection of the HC104A structure revealed it had significant similarity to the compound
212 virstatin (31). Virstatin is an anti-virulence compound that inhibits *Vibrio cholera* cholera toxin
213 production by targeting the transcription regulator ToxT (31). Virstatin inhibits ToxT protein
214 dimerization and subsequently interferes with DNA binding, thereby inhibiting the transcription of
215 downstream genes involved in toxin production. Based on the similarity of chemical structure
216 between HC104A and virstatin, we hypothesized that HC104A may be targeting DosR, and
217 interfering with DNA binding. To test this hypothesis, an electrophoretic mobility shift assay
218 (EMSA) was employed to investigate the impact of HC104A on DosR DNA binding.
219 Recombinant DosR protein, ranging from 0.5 μM to 4 μM, was treated with 40 μM HC104A or a
220 DMSO control and tested for binding to fluorescently labeled *hspX* promoter DNA. In the DMSO
221 treated control, DosR bound promoter DNA beginning at a concentration 2 μM DosR protein
222 (Fig. 4a). Treating the reaction containing 2 μM DosR protein with HC104A significantly inhibited
223 DNA binding by ~22-fold compared to DMSO control (Fig. 4b). To further characterize the
224 impact of HC104A on DosR binding of DNA, a dose-response study was performed. Reactions
225 containing 2 μM recombinant DosR proteins were treated with different concentrations of

226 HC104A or virstatin ranging from 1 – 80 μM. HC104A inhibited DosR binding of DNA beginning
227 at 10 μM HC104A. The fraction of free DNA increased as HC104A concentration increased (Fig.
228 3.4c). For example, the fraction of free DNA was 72%, 89%, 92%, 96% and 100% for 20 μM, 30
229 μM, 40 μM, 60 μM and 80 μM HC104A, respectively, whereas DMSO control had 15% free
230 DNA (Fig. 4d). Thus, HC104A significantly inhibits DosR-DNA binding in a dose-dependent
231 manner. Reactions treated with virstatin had no impact on DosR binding of DNA
232 (Supplementary Fig. 5a). Consistent with these observations, virstatin did not have any impact
233 on DosRST signaling in the whole cell Mtb fluorescence reporter assay (Supplementary Fig.
234 5b). These findings support the hypothesis that HC104A may function by inhibiting DosR DNA
235 binding activity and has an activity that is distinct from the related molecule virstatin.
236
237 ***HC106A modulates DosS heme***
238 DosS and DosT have a channel that exposes the heme to the environment and enables
239 interactions with gases (32, 33). This channel is an Archilles heel that can be targeted by small
240 molecules. Previously, it was shown that the artemisinin modulates DosS/T by oxidizing and
241 alkylating heme carried by the kinases (27). UV-visible spectroscopy studies were conducted to
242 examine if HC106A modulated DosS heme. Recombinant DosS was purified from *E. coli*,
243 degassed and the change of DosS heme spectrum was monitored under anaerobic conditions
244 by UV-visible spectroscopy. Treating DosS with the reducing agent dithionite (DTN) caused the
245 Soret peak to shift to 430 nm as shown previously (13, 27). HC106A was added to the reaction
246 following DTN treatment to observe the impact on the DosS heme UV-visible spectrum.
247 HC106A caused the DosS Soret peak to immediately shift to 422 nm, where the peak was
248 stably maintained for 2 h (Fig. 5a). This spectrum shift is different from artemisinin, where under
249 identical conditions, artemisinin causes the DosS Soret peak to gradually shift back to the

250 oxidized state at 403 nm (27). These findings show that HC106A may also interact with sensor
251 kinase heme, but via a mechanism that is distinct from artemisinin-heme interactions.

252 The Soret peak at 422 nm is consistent with previously described spectra that are
253 observed when DosS heme interacts with NO or CO (13). To confirm this observation, DosS
254 was treated with 100 μM CORM-2 (a CO donor) which caused a shift of the Soret peak to 422
255 nm, similar to what was observed for HC106A (Fig. 5b). This finding supports a hypothesis that
256 HC106A may also be directly binding to the heme. Notably, CO activates DosS kinase function,
257 whereas HC106A functions to inactivate the regulon, demonstrating that the impact of heme
258 binding by CO or HC106A has differing impacts on the sensor kinase switch.

259 Amino acid substitutions in the channel exposing the DosS heme to the environment,
260 such as DosS E87L or G117L, can limit access of artemisinin to modulate heme (27). To
261 support the hypothesis that HC106A directly targets DosS heme, we tested the impact of these
262 amino acid substitutions on HC106A/DosS heme interactions. Treating DosS(E87L) with
263 HC106A exhibited a profile similar to wild type DosS with the Soret peak shifting to 422 nm
264 (Supplementary Fig. 6). However, DosS(G117L) had no change to the overall spectrum after
265 HC106A treatment (Fig. 3.5c). This finding indicates that DosS(G117L) is resistant to HC106A,
266 and confirms that HC106A accesses the heme via a similar mechanism as artemisinin.

267 To confirm DosS is a target of HC106A in Mtb, we examined the impact of
268 overexpressing DosS protein in Mtb. If DosS is the target of HC106A, overexpression may
269 reduce the effectiveness of HC106A. WT DosS protein was constitutively expressed from the
270 *hsp60* promoter in Mtb. The vector control showed that both *hspX* and *tgs1* genes were
271 downregulated by HC106A by 2331- and 3470-fold, respectively (Fig. 5d). Overexpressing
272 DosS provided significant resistance to HC106A, with *hspX* and *tgs1* showing 23- and 16.5-fold
273 less inhibition, respectively, relative to the empty vector control This observation of resistance in
274 Mtb is consistent with the biochemical data supporting the view that DosS is a direct target of
275 HC106A.

276

277 ***Synergistic interactions between DosRST inhibitors***

278 With multiple distinct inhibitory activities of the HC101A, HC102A, HC103A, HC104A
279 and HC106A, we sought to examine if potentiating or antagonistic interactions existed between
280 the molecules, when targeting the DosRST pathway. To examine these interactions,
281 checkboard assays were performed with pairwise comparisons of artemisinin (HC101A),
282 HC102A, HC103A, HC104A and HC106A. CDC1551 (*hspX'::*GFP) was treated with
283 combinations of two compounds ranging from 50 μM to 0.08 μM in 96-well plates. DosR-driven
284 GFP fluorescence and optical density were measured following 6 d of treatment. The
285 Combination Index (CI) was calculated for each drug pair based on the Chou-Talalay method in
286 the CompuSyn software package (34, 35), where CI values of < 1, = 1 and >1 indicate
287 synergistic, additive or antagonistic interactions, respectively. Among all 64 compound pairs,
288 artemisinin combined with HC102A, HC103A, HC104A and HC106, showed 46, 49, 41, and 50
289 combinations that have CI <1, respectively (Fig. 3.6). Notably, some CI values are below 0.1
290 when artemisinin was paired with HC102A, HC103A or HC106A combinations. Example dose
291 response curves illustrate these synergistic interactions (Fig. 6). Several other pairwise
292 comparisons also demonstrated synergy (Supplementary Fig. 7), however, in general, these
293 interactions had CI between 1 and 0.1, supporting weaker synergistic interactions, as compared
294 to combinations with artemisinin. Overall, these studies provide the evidence that the inhibitors
295 function by distinct mechanisms and may be combined to improve potency.

296

297 ***Structure-activity relationship study for HC104A and HC106***

298 We conducted a catalog search for HC104 and HC106 analogs and obtained 10
299 commercial analogs for each series to define initial structure activity relationships (SAR). For
300 HC104A we observed that a bromine in the 5-position is required for activity and that the R2
301 dimethylamine group is not required (Supplementary Table 1). For example, HC104B is

302 identical to HC104A except for the removal of the bromine (R1), which results in a complete loss
303 of activity in the whole cell assay. Whereas, replacement of the R2 group with a methyl
304 (HC104G) results in an active compound, although ~5-fold less active than HC104A. Although
305 not highly potent, its ligand efficiency, cLogD and druglikeness are in the range of what would
306 be considered acceptable to good as a starting point for further manipulation. For HC106A
307 (Table 1), catalog SAR work led to new understandings of the nature of the series. We first
308 found that the simple removal of an ortho chloro on the "A" ring of HC106A leads to ~ 2-fold
309 enhanced activity, with an EC_{50} in the whole cell Mtb assay for DosRST inhibition of 1.33 μM
310 (HC106F). It was also found that the use of an alternative isomer of the isoxazole had no
311 detectable activity (HC106C).
312
313 To further understand the SAR of the HC106 series, additional analogs were
314 synthesized to examine the need of the central urea functionality and whether modifications
315 can be tolerated (Table 1). A pyridyl analog (MSU-41425), designed to replace the isoxazole
316 also demonstrated no activity as was the symmetrical 4-chloroaniline derived urea (MSU-
317 41324). However, the bis-isoxazole urea (MSU-39444) provides an EC_{50} of 1.7 μM, indicating
318 that the isoxazole is important for function. Isoxazoles are unique among heterocycles in that
319 they exist in multiple tautomeric forms as supported by initial NMR studies (36). We next
320 explored the need of one of the -NHs of the urea, capping it with a methyl (MSU-39451),
321 integrating it into a ring for conformational restriction (MSU-39453), and replacing with a
322 methylene unit (MSU-39449). In all cases, reduced activity (0.5 - 1 log) was observed but not
323 all activity was lost. Thus, HC106A is a potent whole cell inhibitor of the DosRST pathway,
324 with flexibility to be improved via SAR.
325 To further test the SAR, we conducted a Topliss Tree evaluation of the "A-ring" aniline
326 (Table 20)(37). To reliably prepare the derivatives, we explored and established a general
327 preparation (Supplementary Fig. 8). This route is preferred relative to alternative approaches

328 for its cleanliness, yields and ease of purification, usually by trituration. It is also anticipated
329 that it will allow access to future derivatives. Using HC106F and HC106A as starting points,
330 we prepared the 3,4-diclorochloro and 3-chloro derivatives (MSU-39452 and MSU-39445,
331 respectively). Both the 3- and 4-chloro derivatives demonstrated greater activity than 3,4-
332 dichloro (MSU-39452). We found that replacing the 4-chlorophenyl ring with pyridyl analogs
333 (MSU-39448 and MSU-39450) lead to similar activity. Focusing on 4-position derivatives, we
334 found that fluoro (MSU-39446), bromo (MSU-41464) and methoxy (MSU-39447), as electron
335 p-orbital donating substituents, also lead towards incrementally increased activity. Para-t-butyl
336 phenyl (MSU-41442), provided slightly diminished activity. Electron withdrawing substituents,
337 such as 4-CO_2Me (MSU-4165), 4-trifluoromethyl (MSU-41463) and biphenyl (MSU-41443)
338 saw activity similar to the 4-chlorophenyl derivative (HC106F). Overall, several analogs were
339 discovered with significantly ~4-fold enhanced potency, with several inhibitors having whole
340 cell DosRST inhibitory EC_{50} below 1 μM, including EC_{50} of 0.63 μM, 0.61 μM, 0.54 μM and
341 0.75 μM for MSU-33189, -39447, -39446, and -39455, respectively. The parent analog
342 HC106A had an EC_{50} of 2.48 μM.

343 There appears to be little sensitivity, positive or negative, for electron-drawing
344 substituents other than the biphenyl derivative (MSU-41443), which is likely the result of
345 negative steric interactions in the binding domain. Additional derivatives (replacement of
346 dichlorophenyl) were also prepared to further probe the size and nature of the binding domain.
347 We began by replacing the chlorophenyl ring of HC106F with benzyl- (MSU-41462), isobutyl-
348 (MSU-41542), cyclopentyl- (MSU-41546) and cyclohexyl- (MSU-42002) analogs. All analogs
349 demonstrated similar activities, relative to HC106F and the simple phenyl analog (MSU-
350 33189), suggesting flexibility of fragments that could bind in this domain.

351 Kinetic solubility assays were conducted for selected analogs and all exhibited
352 excellent aqueous solubility greater than >100 μM, except for MSU-41443 (Table 2). This
353 finding shows that the urea group present in the HC106A does not have a detrimental impact

354 on HC106 aqueous solubility. All of the tested deriviatives also demonstrated favorable
355 mouse microsomal stability, including. Overall, the nanomolar whole cell potency, flexible
356 SAR, good microsomal stability and excellent solubility, confirm that the HC106 series is a
357 suitable series for continued optimization to identify a drug-like lead.

358 DosRST is a two-component regulatory system required for Mtb environmental sensing,
359 adaptation, and persistence. By using a fluorescent reporter strain CDC1551 (*hspX'::GFP*), we
360 have previously discovered small molecule inhibitors of DosRST, named HC101A-HC106A,
361 from the whole-cell phenotypic HTS. Here, we report the characterizations of HC104A and
362 HC106A as DosRST inhibitors. Both compounds downregulated genes in the DosR regulon,
363 and inhibited TAG biosynthesis. HC106A also reduced Mtb survival during NRP.

364 In a UV-visible spectroscopy assay, we observed that HC106A interacts with the heme
365 of sensor kinase DosS. The UV-visible spectrum of HC106A-treated DosS is similar to those of
366 CO- or NO-treated DosS. The overlap between the CO and HC106A spectra supports that
367 HC106A may also directly bind to the heme of DosS. Interestingly, CO activates sensor kinases,
368 whereas HC106A inhibits them. This could be due to the difference in conformational changes
369 induced by CO and HC106A, or binding of HC106A may lock the sensor kinases into an inactive
370 state. Furthermore, the DosS G117L substitution in recombinant DosS blocks the heme
371 exposing channel and provides resistance to HC106A. This means that, similar to artemisinin,
372 this channel is also important for the activity of HC106A. These findings provide additional
373 evidence that the heme-exposing channel in DosS/T can be exploited by small molecules to
374 inhibit the heme from sensing signals and to disrupt signal transduction of a two-component
375 regulatory system. To our knowledge, these two distinct mechanisms of actions are novel
376 mechanisms to inhibit the DosRST pathway.

377 Mechanistic studies via EMSA indicates that HC104A may function by targeting DosR
378 and inhibiting DosR DNA binding. Virstatin had no effect on DosR DNA binding and no impact
379 on the DosRST signaling in whole cells, showing that although both compounds share a similar

380 structure, they function by distinct mechanisms. From the catalog SAR study, we found that the
381 bromine group is required for the compound. Virstatin does not have the bromine, and the R-
382 group is butyric acid instead of dimethylamine. These two differences are enough to differentiate
383 the activity of the compounds. Moreover, transcriptional profiling shows that the most repressed
384 genes by HC104A are from the DosR regulon, providing additional evidence that HC104A is
385 somewhat selective for specific DosR regulated genes. Interestingly, the genes most
386 downregulated by HC104A, including *hspX*, *Rv2030c*, *pfkB*, and *Rv2028c*, are from the same
387 operon under control of *hspX* promoter, which is strongly induced by DosR in hypoxia. This
388 result suggests that HC104A is more specific to target *hspX* operon genes as compared to other
389 DosR regulated genes. This finding leads to the speculation that HC104A may be more efficient
390 to prevent DosR binding to the *hspX* promoter than the other DosR promoters. HC104A may fit
391 better in the pocket in the interface of DosR-*hspX'* complex. This postulation also supports the
392 idea that HC104A may not have an impact on DosR protein dimerization, which would lead to
393 universal downregulation of DosR-regulated genes. Detailed characterizations of HC104A on
394 inhibiting DosR dimerization and promoter binding specificity is the subject of ongoing
395 characterizations.

396 This study together with the previous report reveals multiple distinct inhibitory
397 mechanisms for the five compounds, HC101A-104A, HC106A. Four out five compounds,
398 HC101A-HC103A and HC106A, are proposed to function by targeting the sensor kinases
399 DosRST. Furthermore, these four compounds are effective at decreasing Mtb survival during
400 NRP in hypoxic-shift down assay. In contrast, the compound targeting DosR, HC104A, had no
401 impact on Mtb survival during NRP. This result is consistent with a previous report that showed
402 only the Δ*dosS* mutant exhibits a survival defect in the C3HeB/FeJ mouse model (22). Notably,
403 the *dosR* mutant strain used in our study is also lacking *dosS* expression due to polar impacts of
404 the deletion, supporting the hypothesis that the reduced survival during NRP may be dependent
405 on DosS. Alternatively, we noted that HC104A only inhibits a portion of the DosR regulon with

406 only 26 genes being downregulated. This finding suggests that the DosR regulated genes that
407 are inhibited by HC104A (Fig. 2, and Supplementary Dataset 1, 3) are not required for DosRST-
408 dependent persistence during NRP or not sufficiently inhibited to have an impact on survival.

409 The transcriptional profiling data showed off-target impacts in the treated *dosR* mutant
410 strain. These effects may be due to inhibition of DosS/T signaling that functions independent of
411 the response regulator. Several recent studies have demonstrated the occurrence of cross-
412 interactions between histidine kinases and response regulators in Mtb. For instance, Lee *et al.*
413 shows that DosT can interact with the other non-cognate response regulators, including NarL
414 and PrrA (38). Our transcriptional profiling of the compound treated *dosR* mutant strain
415 suggests that some genes downregulated by HC101A, HC103A and HC106A may be DosS-
416 dependent but DosR-independent (Supplementary Fig 9). In the prior study, six genes are
417 similarly regulated between artemisinin and HC103A in the treated *dosR* mutant strain, including
418 Rv0260c that encodes a putative response regulator (27). HC106A and HC103A share four
419 differentially regulated genes in the *dosR* mutant, including *argC*, *argJ*, *argB*, and *argF*, which
420 are genes involved in arginine biosynthesis. Our data presented here and in the literature point
421 to the possibility that DosST modulate gene expression independently of DosR.

422 The synergy studies show significant synergistic interactions between artemisinin,
423 HC102A, HC103A, HC104, or HC106A. Moreover, artemisinin exhibited the greatest synergistic
424 activities with HC102A, HC103A or HC106A, indicating that inhibition of histidine kinases by a
425 second inhibitor can lead to synergistic inhibition of the DosRST pathway. This interaction could
426 be due to both sensor kinases being required for full induction of the DosR regulon, where DosT
427 responds early during hypoxia and DosS further induces the regulon at later times (39), and it is
428 possible that the inhibitors have different affinities for DosS or DosT. Thus, multiple inhibitors
429 could inhibit both DosS and DosT better than an inhibitor alone. Interestingly, artemisinin shows
430 the greatest synergism with HC106A. Both compounds are proposed to target the heme of

431 DosS/T, but through different mechanisms. This finding shows that both inhibitors can enter the
432 channel of DosST to interact with the heme and do so without antagonizing interactions.

433 The identification of new antibacterial agents and tuberculosis drugs has been
434 associated with the realization that these compounds can occupy a different region of chemical
435 space relative to drugs in most other therapeutic areas. Series HC106 is easily in the range of
436 the characteristics for compounds currently in use or in development as anti-TB compounds.
437 Series HC104 needs further exploration to fully assess its suitability. The physicochemical
438 properties of a drug, such as solubility and permeability, impact its oral bioavailability as these
439 factors influence absorption, distribution, metabolism, and excretion. Series HC106
440 demonstrates excellent aqueous solubility (Table 2, with compounds generally having solubility
441 >100 μM). The melting points of most of the compounds in the series and the corresponding
442 cLogP are also supportive appropriate solubility. The ability of an anti-TB drug to reach its target
443 site is greatly hampered by the highly impermeable Mtb cell envelope. Both series (HC104 and
444 HC106) demonstrate low micromolar and nanomolar whole cell EC_{50} values, suggesting
445 adequate cell wall permeability. SAR studies of HC106 show that there remain significant
446 opportunities for optimization of HC106 for potency and drug properties and future studies will
447 be focused on such optimizations.

448

449 **Methods**

450 ***Bacterial strains and growth conditions.*** Mtb CDC1551, CDC1551 (Δ*dosR*) strains were
451 used in this study. All cultures were grown at 37°C and 5% CO_2 in 7H9 Middlebrook medium
452 supplemented with 10% OADC (oleic acid albumin dextrose catalase) and 0.05% Tween-80 in
453 standing, vented tissue culture flasks, unless stated otherwise.

454

455 ***EC_{50} assays.*** The assay was performed as previously described (27). Briefly, the (*hspX'::GFP*)

456 reporter strain culture was diluted to an OD_{600} of 0.05 in fresh 7H9 media, pH 7.0, and 200 μL of
457 diluted culture was aliquoted in clear-bottom, black, 96-well plates (Corning). Cells were treated
458 with an 8-point (2.5-fold) dilution series ranging from 200 μM – 0.32 μM. For the structure
459 relationship studies for the HC106 series, a 12-point (2.5-fold) dilution series of HC106 analogs
460 ranging from 200 μM – 8.4 nM were used. GFP fluorescence and optical density were
461 measured following 6 d incubation. Percentage fluorescence and growth inhibitions were
462 normalized to a rifampin-positive control (100% inhibition) and DMSO-negative control (0%
463 inhibition). EC_{50} values were calculated for each compound using GraphPad Prism software
464 package (version 6). Each experiment was performed with two technical replicates per plate and
465 two biological replicates, and the error bar represents the s.d. of the biological replicates.
466 Experiments were performed twice with similar results.
467
468 ***Transcriptional profiling and data analysis.*** Transcriptional profiling studies were conducted
469 as previously described in Zheng *et al.* (27). Briefly, CDC1551 or CDC1551 (Δ*dosR*) cultures
470 were treated with 40 μM HC104A, HC106A or DMSO control for 6 d. The starting OD_{600} was 0.1
471 in 8 mL of 7H9 medium in standing T25 vented tissue culture flasks. Bacterial growth consumes
472 oxygen and stimulates the DosRST pathway. The total bacterial RNA from two biological
473 replicates was isolated and prepared for sequencing as previously described (40). The RNA-seq
474 data were processed and analyzed using the SPARTA software package (41). Sequencing data
475 are available at the GEO Database (Accession GSE115892).
476
477 ***Real time-PCR assays.*** The vitamin C and NO assays were performed as previously described
478 (27). Briefly, cultures at an OD_{600} of 0.6 were pretreated with 80 μM HC104A, HC106A or a
479 DMSO control for 24 h, and induced with 50 μM DETA-NONOate or 20 mM vitamin C for 2 h.
480 For the HC106A resistance assays, CDC1551 was transformed with the empty replicating

481 plasmid pVV16 or the plasmid expressing *dosS* from the strong *hsp60* promoter (pVV16-DosS),
482 and treated with 20 μM HC106A for 6 d. Total bacterial RNA was isolated and differential gene
483 expression of DosR-regulated genes, including *hspX* and *tgs1*, was quantified. The experiment
484 was performed in three technical replicates and error bars represent the s.d from the mean. The
485 experiment was repeated twice with similar results. To examine Mtb gene expression in
486 macrophages, murine bone-marrow derived macrophages were isolated as previously
487 described (42) and seeded in T75 vented, tissue culture flasks. Macrophages were infected with
488 CDC1551 with multiplicity of infection ratio of 1:20 as previously described (42). After infection,
489 the flasks were treated with 40 μM HC104A or HC106A or DMSO for 48 h, with three individual
490 flasks for each treatment. Total bacterial RNA was isolated after treatment, and the transcripts
491 of DosR-controlled genes (*hspX* and *tgs1*) were quantified in RT-PCR. The experiment was
492 conducted with three biological replicates. The error bar represents the s.d. of the biological
493 replicates.
494
495 ***TAG biosynthesis.*** The lipid labelling and TAG TLCs were performed as previously described
496 (27). Briefly, CDC1551 was cultured at an initial OD_{600} of 0.1 and radiolabeled with 8 μCi of [1,2-
497 ^{14}C] sodium acetate in T25 vented tissue culture flasks. The cultures were treated with 40 μM
498 HC104A, HC106A or DMSO for 6 d at 37°C. CDC1551 (Δ*dosR*) and *dosRS* complement strains
499 were also examined. Total lipids were extracted and ^{14}C incorporation was determined by
500 scintillation counting. 20,000 c.p.m. of total lipids were analyzed by TLC using silica gel 60
501 aluminum sheets (EMD Millipore). To determine TAG accumulation, the lipids were developed
502 in hexane-diethyl ether-acetic acid (80:20:1; vol/vol/vol) solvent system. The TLC was exposed
503 to a phosphor screen for 3 d, and imaged on a Typhoon imager and TAG was quantified using
504 ImageJ software (43). The experiment was repeated twice with similar results, and the error bar
505 represents the s.d. of two biological replicates.

506

507 ***NRP survival assays.*** Survival during NRP was examined using the hypoxic shift down assays
508 as previously described (27, 44). Briefly, CDC1551 cells were treated with 40 μM HC104A,
509 HC106A or DMSO control in a 24-well plate (1 mL/well). CDC1551 (Δ*dosR*) and *dosRS*
510 complement strains were also examined. Plates were incubated in an anaerobic chamber (BD
511 GasPak) for 12 d. It took 48 h for cultures to become anaerobic, as monitored by a methylene
512 blue control. Bacterial CFUs were numerated on 7H10 agar plates following incubation. The
513 experiment was repeated twice with similar results.

514

515 ***DosR protein purification.*** DosR full length protein was purified as previously described (45).
516 Briefly, the *dosR* gene (Rv3133c) was cloned into pET15b (Novagen Darmstadt, Germany)
517 using the primer set: forward primer 5'-TTTCATATGGTGGTAAAGGTCTTCTTGGTCGATGAC-
518 3'; reverse primer 5'-TTTGGATCCTCATGGTCCATCACCGGGTGG-3'. The His_6-DosR protein
519 was expressed in *E. coli* BL21(DE3) strain. The culture was grown to OD_{600} 0.5-06, and induced
520 with 1 mM IPTG for 6.5 h at 29°C. The cell pellet was suspended in lysis buffer (20 mM Tris-
521 HCl, pH 8.0, 10% glycerol, 500 mM NaCl, 0.5 mg/ml lysozyme and 0.1 mg/ml PMSF), and
522 incubated at 37°C for 30 min. The soluble fraction of lysate was collected after centrifugation
523 and applied to a TALON metal affinity Co^{2+} column (Clontech). The column was washed twice
524 with washing buffer (20 mM Tris-HCl, pH 8.0, 10% glycerol, 500 mM NaCl) without imidazole,
525 then with 20 mM imidazole. The protein was eluted with the same buffer containing 300 mM
526 imidazole. The fractions with the most DosR protein (as determined by SDS-PAGE) were
527 pooled together for dialysis in 25 mM Tris-HCl, pH 8.0. The final protein concentration was
528 determined using a Qubit kit (Invitrogen).

529

530 ***Electrophoretic mobility assay.*** The assay is fluorescence-based using 6-carboxyfluorescein
531 (6FAM) labeled 385 bp probe from the *hspX* promoter. In designing the primer set, 6FAM was
532 added to the 5' ends of forward and reverse primers. The *hspX* probe was synthesized via PCR
533 using the primer set: forward primer 5'-6FAM-CAACTGCACCGCGCTCTTGATG-3'; reverse
534 primer 5'-6FAM-CATCTCGTCTTCCAGCCGCATCAAC-3'. The probe was purified by Qiagen
535 PCR purification kit. The DosR protein was pre-phosphorylated in 10 μL of phosphorylation
536 buffer (40 mM Tris-HCl, pH 8.0, 5 mM $MgCl_2$, 50 mM lithium potassium acetyl phosphate), and
537 incubated at room temperature for 30 min. The protein was then transferred to binding buffer in
538 a final volume of 20 μL (final concentration, 25 mM Tris-HCl, pH 8.0, 0.5 mM EDTA, 20 mM KCl,
539 6 mM $MgCl_2$, 10 nM probe, 1 μg poly-dI-dC (Sigma Aldrich)), and treated with HC104A or an
540 equal volume of DMSO or virstatin (Santa Cruz Biotech). Two different assays were performed.
541 Firstly, different DosR protein concentrations from 0.5 μM to 4 μM were treated with 40 μM.
542 Second, dose response assays were performed with 2 μM DosR treated with different
543 concentrations of HC104A or virstatin from 1 μM to 80 μM. After incubating on ice for 30 min,
544 the reactions were terminated by adding 1 μL 80% glycerol, and loaded on a native 5%
545 Tris/Borate/EDTA (TBE) polyacrylamide gel. The gel was run at 50 V, for 5-6 h at 4°C in 1X TBE
546 buffer, and was imaged using a Typhoon scanner with appropriate filters that can detect
547 florescence at excitation = 495 nm, emission = 520 nm. Binding of the unbound probe was
548 quantified using ImageJ (43). The assay was repeated at least twice with similar results. The
549 error bar represents the s.d. of two biological replicates.
550
551 ***UV-visible spectroscopy assay.*** DosS and mutant proteins were purified and analyzed as
552 previously described (27). Briefly, 7.5 μM of recombinant DosS protein was deoxygenated with
553 argon gas in a sealed cuvette. The protein was reduced with 400 μM DTN for 20 min. The
554 reaction was then treated with 100 μM HC106A, 400 μM HC104A, 100 μM CORM-2

555 (tricarbonyldichlororuthenium (II) dimer) or equal volume of DMSO. The UV-visible spectra were
556 recorded for kinetic changes over 2 h. The experiment was repeated at least twice with similar
557 results.
558
559 ***Checkerboard synergy studies.*** The reporter strain CDC1551 (*hspX::GFP*) was treated with
560 pairs of DosRST inhibitors from 50 μM – 0.08 μM in 96-well plates, including HC101A-HC104A
561 and HC106A. GFP fluorescence and OD_{600} were measured after 6 d incubation. The
562 percentage of fluorescence inhibition (FI) and growth inhibition were calculated for each drug
563 pair, with limited growth inhibition observed. The FI data was utilized for further analysis of
564 interactions using CompuSyn software (34). The Combination Index (CI) value was calculated
565 for each drug pair according to the Chou-Talalay method, which is based on the Median-Effect
566 equation derived from the Mass-Action Law principle (35, 46). The resulting CI values provide
567 quantitative determination of drug interactions, including synergism (CI < 1), additive effect (C =
568 1), and antagonism (C > 1).
569
570 ***Autophosphorylation assay.*** The DosS autophosphorylation assay was performed as
571 previously described (27). Recombinant DosS protein was treated with 10 μM, 20 μM or 40 μM
572 of HC104A, or HC106A. DMSO and 40 μM HC103A were also included as positive and
573 negative controls, respectively.
574
575 ***Kinetic solubility assay.*** The assay was performed with 7-point (2-fold) dilutions from 200 μM -
576 3.125 μM for HC106 analogs. Mebendazole, benxarotene and aspirin were also included as
577 controls. The drug dilutions were added to PBS, pH 7.4, with the final DMSO concentration of
578 1%, and incubated at 37 °C for 2 h. The absorbance at 620 nm was measured for each drug

579 dilution to estimate of the compound solubility. Three replicates were examined for each
580 dilution.
581
582 **Acknowledgements**
583 The MSU RTSF provided technical support for the RNA-seq library preparation and sequencing.
584 This project was supported by start-up funding and a Molecular Discovery Grant from Michigan
585 State University, AgBioResearch, a grant from the NIH-NIAID (R21AI105687) and Grand
586 Challenges Explorations grants from the Bill and Melinda Gates Foundation (OPP1059227 and
587 OPP1119065).
588 **Author Contributions**
589 H.Z., E.E. and R.B.A conceived the experiments. H.Z. performed the Mtb physiology and
590 biochemistry experiments. B.A. synthesized the analogs. E.E. directed the medicinal chemistry
591 optimizations. H.Z, E.E. and R.B.A wrote the manuscript.
592
593 **Disclosures**
594 RBA is the founder and owner of Tarn Biosciences, Inc., a company that is working to develop
595 new TB drugs.

596 **References**
597
598 1. Boon C & Dick T (2012) How *Mycobacterium tuberculosis* goes to sleep: the dormancy
599 survival regulator DosR a decade later. *Future microbiology* 7(4):513-518.
600 2. Rustad TR, Sherrid AM, Minch KJ, & Sherman DR (2009) Hypoxia: a window into
601 Mycobacterium tuberculosis latency. *Cell Microbiol* 11(8):1151-1159.
602 3. Wayne LG & Sohaskey CD (2001) Nonreplicating persistence of mycobacterium
603 tuberculosis. *Annu Rev Microbiol* 55:139-163.
604 4. Mehra S*, et al.* (2015) The DosR Regulon Modulates Adaptive Immunity and Is Essential
605 for Mycobacterium tuberculosis Persistence. *American journal of respiratory and critical*
606 *care medicine* 191(10):1185-1196.
607 5. Hudock TA*, et al.* (2017) Hypoxia sensing and persistence genes are expressed during
608 the intragranulomatous survival of *Mycobacterium tuberculosis*. *American journal of*
609 *respiratory cell and molecular biology* 56(5):637-647.
610 6. Dasgupta N*, et al.* (2000) Characterization of a two-component system, devR-devS, of
611 *Mycobacterium tuberculosis*. *Tubercle and lung disease : the official journal of the*
612 *International Union against Tuberculosis and Lung Disease* 80(3):141-159.
613 7. Park HD*, et al.* (2003) Rv3133c/dosR is a transcription factor that mediates the hypoxic
614 response of Mycobacterium tuberculosis. *Mol Microbiol* 48(3):833-843.
615 8. Saini DK*, et al.* (2004) DevR-DevS is a bona fide two-component system of
616 *Mycobacterium tuberculosis* that is hypoxia-responsive in the absence of the DNA-
617 binding domain of DevR. *Microbiology (Reading, England)* 150(Pt 4):865-875.
618 9. Voskuil MI*, et al.* (2003) Inhibition of respiration by nitric oxide induces a Mycobacterium
619 tuberculosis dormancy program. *J Exp Med* 198(5):705-713.
620 10. Kumar A*, et al.* (2008) Heme oxygenase-1-derived carbon monoxide induces the
621 Mycobacterium tuberculosis dormancy regulon. *J Biol Chem* 283(26):18032-18039.
622 11. Lee JM*, et al.* (2008) O2- and NO-sensing mechanism through the DevSR two-
623 component system in *Mycobacterium smegmatis*. *Journal of bacteriology* 190(20):6795-
624 6804.
625 12. Sousa EH, Tuckerman JR, Gonzalez G, & Gilles-Gonzalez MA (2007) DosT and DevS
626 are oxygen-switched kinases in *Mycobacterium tuberculosis*. *Protein science : a*
627 *publication of the Protein Society* 16(8):1708-1719.
628 13. Kumar A, Toledo JC, Patel RP, Lancaster JR, Jr., & Steyn AJ (2007) Mycobacterium
629 tuberculosis DosS is a redox sensor and DosT is a hypoxia sensor. *Proc Natl Acad Sci*
630 *U S A* 104(28):11568-11573.
631 14. Ioanoviciu A, Yukl ET, Moenne-Loccoz P, & de Montellano PR (2007) DevS, a heme-
632 containing two-component oxygen sensor of *Mycobacterium tuberculosis*. *Biochemistry*
633 46(14):4250-4260.
634 15. Kim MJ, Park KJ, Ko IJ, Kim YM, & Oh JI (2010) Different roles of DosS and DosT in the
635 hypoxic adaptation of Mycobacteria. *J Bacteriol* 192(19):4868-4875.
636 16. Rao SP, Alonso S, Rand L, Dick T, & Pethe K (2008) The protonmotive force is required
637 for maintaining ATP homeostasis and viability of hypoxic, nonreplicating Mycobacterium
638 tuberculosis. *Proc Natl Acad Sci U S A* 105(33):11945-11950.
639 17. Adams KN*, et al.* (2011) Drug tolerance in replicating mycobacteria mediated by a
640 macrophage-induced efflux mechanism. *Cell* 145(1):39-53.
641 18. Grant SS, Kaufmann BB, Chand NS, Haseley N, & Hung DT (2012) Eradication of
642 bacterial persisters with antibiotic-generated hydroxyl radicals. *Proceedings of the*
643 *National Academy of Sciences of the United States of America* 109(30):12147-12152.
644 19. Leistikow RL*, et al.* (2010) The Mycobacterium tuberculosis DosR regulon assists in
645 metabolic homeostasis and enables rapid recovery from nonrespiring dormancy. *J*
646 *Bacteriol* 192(6):1662-1670.

647 20. Converse PJ*, et al.* (2009) Role of the dosR-dosS two-component regulatory system in
648 Mycobacterium tuberculosis virulence in three animal models. *Infect Immun* 77(3):1230-
649 1237.
650 21. Gautam US, Mehra S, & Kaushal D (2015) *in-vivo* gene signatures of *Mycobacterium*
651 *tuberculosis* in C3HeB/FeJ Mice. *PloS one* 10(8):e0135208.
652 22. Gautam US*, et al.* (2015) DosS is required for the complete virulence of *Mycobacterium*
653 *tuberculosis* in mice with classical granulomatous lesions. *American journal of*
654 *respiratory cell and molecular biology* 52(6):708-716.
655 23. Deb C*, et al.* (2009) A novel in vitro multiple-stress dormancy model for Mycobacterium
656 tuberculosis generates a lipid-loaded, drug-tolerant, dormant pathogen. *Plos One*
657 4(6):e6077.
658 24. Basak A*, et al.* (2017) Antimicrobial peptide-inspired NH125 analogues: bacterial and
659 fungal biofilm-eradicating agents and rapid killers of MRSA persisters. *Organic &*
660 *biomolecular chemistry* 15(26):5503-5512.
661 25. Abramovitch RB (2018) Mycobacterium tuberculosis Reporter Strains as Tools for Drug
662 Discovery and Development. *IUBMB Life* 70(9):818-825.
663 26. Johnson BK & Abramovitch RB (2017) Small Molecules That Sabotage Bacterial
664 Virulence. *Trends in pharmacological sciences* 38(4):339-362.
665 27. Zheng H*, et al.* (2017) Inhibitors of Mycobacterium tuberculosis DosRST signaling and
666 persistence. *Nature chemical biology* 13(2):218-225.
667 28. Daniel J*, et al.* (2004) Induction of a novel class of diacylglycerol acyltransferases and
668 triacylglycerol accumulation in *Mycobacterium tuberculosis* as it goes into a dormancy-
669 like state in culture. *Journal of bacteriology* 186(15):5017-5030.
670 29. Sirakova TD*, et al.* (2006) Identification of a diacylglycerol acyltransferase gene involved
671 in accumulation of triacylglycerol in *Mycobacterium tuberculosis* under stress.
672 *Microbiology (Reading, England)* 152(Pt 9):2717-2725.
673 30. Baek SH, Li AH, & Sassetti CM (2011) Metabolic regulation of mycobacterial growth and
674 antibiotic sensitivity. *PLoS Biol* 9(5):e1001065.
675 31. Hung DT, Shakhnovich EA, Pierson E, & Mekalanos JJ (2005) Small-molecule inhibitor
676 of Vibrio cholerae virulence and intestinal colonization. *Science* 310(5748):670-674.
677 32. Podust LM, Ioanoviciu A, & Ortiz de Montellano PR (2008) 2.3 A X-ray structure of the
678 heme-bound GAF domain of sensory histidine kinase DosT of Mycobacterium
679 tuberculosis. *Biochemistry* 47(47):12523-12531.
680 33. Cho HY, Cho HJ, Kim YM, Oh JI, & Kang BS (2009) Structural insight into the heme-
681 based redox sensing by DosS from Mycobacterium tuberculosis. *J Biol Chem*
682 284(19):13057-13067.
683 34. Chou T & Martin N (2005) CompuSyn for drug combinations: PC software and user's
684 guide: a computer program for quantitation of synergism and antagonism in drug
685 combinations, and the determination of IC50 and ED50 and LD50 values).
686 35. Chou TC & Talalay P (1984) Quantitative analysis of dose-effect relationships: the
687 combined effects of multiple drugs or enzyme inhibitors. *Adv Enzyme Regul* 22:27-55.
688 36. Boulton AJ & Katritzky AR (1961) The tautomerism of heteroaromatic compounds with
689 five-membered rings—I: 5-hydroxyisoxazoles-isoxazol-5-ones. *Tetrahedron* 12(1):41-50.
690 37. Topliss JG (1972) Utilization of operational schemes for analog synthesis in drug design.
691 *Journal of medicinal chemistry* 15(10):1006-1011.
692 38. Lee HN, Jung KE, Ko IJ, Baik HS, & Oh JI (2012) Protein-protein interactions between
693 histidine kinases and response regulators of *Mycobacterium tuberculosis* H37Rv.
694 *Journal of microbiology (Seoul, Korea)* 50(2):270-277.
695 39. Honaker RW, Leistikow RL, Bartek IL, & Voskuil MI (2009) Unique roles of DosT and
696 DosS in DosR regulon induction and Mycobacterium tuberculosis dormancy. *Infect*
697 *Immun* 77(8):3258-3263.

698 40. Baker JJ, Johnson BK, & Abramovitch RB (2014) Slow growth of Mycobacterium
699 tuberculosis at acidic pH is regulated by phoPR and host-associated carbon sources.
700 *Mol Microbiol* 94(1):56-69.
701 41. Johnson BK, Scholz MB, Teal TK, & Abramovitch RB (2016) SPARTA: Simple Program
702 for Automated reference-based bacterial RNA-seq Transcriptome Analysis. *BMC*
703 *bioinformatics* 17:66.
704 42. Johnson BK & Abramovitch RB (2015) Macrophage Infection Models for Mycobacterium
705 tuberculosis. *Methods Mol Biol* 1285:329-341.
706 43. Schneider CA, Rasband WS, & Eliceiri KW (2012) NIH Image to ImageJ: 25 years of
707 image analysis. *Nature methods* 9(7):671-675.
708 44. Mak PA*, et al.* (2012) A high-throughput screen to identify inhibitors of ATP homeostasis
709 in non-replicating Mycobacterium tuberculosis. *ACS chemical biology* 7(7):1190-1197.
710 45. Vashist A, Prithvi Raj D, Gupta UD, Bhat R, & Tyagi JS (2016) The alpha10 helix of
711 DevR, the *Mycobacterium tuberculosis* dormancy response regulator, regulates its DNA
712 binding and activity. *The FEBS journal* 283(7):1286-1299.
713 46. Chou TC (2010) Drug combination studies and their synergy quantification using the
714 Chou-Talalay method. *Cancer research* 70(2):440-446.
715
716

717 **Figure Legends**
718
719 **Figure 1. HC104A and HC106A inhibit DosRST reporter fluorescence.** (**a**) Chemical structures of
720 HC104A and HC106A. HC104A (**b**) and HC106A (**c**) inhibited DosR-driven GFP fluorescence
721 signal in a dose-dependent manner, while having minimal impact of Mtb growth. The EC_{50}
722 values of fluorescence inhibition for HC104A and HC106A are 9.8 μM and 2.5 μM, respectively.
723
724 **Figure 2. Transcriptional profiling shows HC104A and HC106A inhibited DosR regulon during**
725 **hypoxia.** Magnitude-amplitude plots showing differential gene expression of Mtb cells treated
726 with 40 μM HC104A (**a**) or HC106A (**b**). The labeled genes represent selected genes that
727 belong to the DosRST regulon. The red dots represent genes with significant differential
728 expression, q<0.05. **(c)** A Venn diagram for the downregulated genes (>2-fold; q< 0.05) of WT
729 CDC1551 treated with HC104A or HC106A compared to that of CDC1551 (Δ*dosR*). (**d**) Venn
730 diagram for downregulated genes (>2-fold; q< 0.05) of CDC1551 (Δ*dosR*) treated with HC104A
731 or HC106A.
732
733 **Figure 3. Inhibition of DosR regulon and persistence-associated physiologies by HC104A and**
734 **HC106A.** (**a**) Inhibition of DosR regulon in murine macrophages infected with Mtb and treated
735 with HC104A and HC106A for 48 h. Bacterial RNA was isolated after incubation, and the
736 differential gene expression of *hspX* and *tgs1* bone-marrow derived were quantified by qRT-
737 PCR. The error bars represent the standard derivation of three biological replicates. (**b**) HC104A
738 and HC106A inhibit DosR regulon induction by vitamin C and NO. Cells were pretreated with
739 the compounds or DMSO for 24 h, and induced with vitamin C or NO for 2 h. Total bacterial
740 RNA was isolated, and the transcripts of DosR-regulated genes, *hspX* and *tgs1*, were quantified
741 by qRT-PCR. The difference in the drug treated samples compared to DMSO treated samples
742 in response to vitamin C or NO are significant with a p-value <0.001 based on a t-test, except

743 the one marked as non-significant (n.s.). The error bars represent the standard deviation of
744 three replicates. The experiment was repeated twice with similar results. (**c**) Inhibition of TAG
745 accumulation of Mtb treated with HC104A or HC106A. Mtb cells were treated with 40 μM of the
746 compounds and labeled with [1,2-^{14}C] sodium acetate for 6 d. Total lipid was isolated and
747 analyzed by TLC. TAG accumulation was quantified from the TLC. The error bars represent the
748 standard derivation of two biological replicates. (**d**) Mtb cell survival during NRP when treated
749 with HC104A or HC106A during NRP. Mtb cells were pretreated with 40 μM of compounds for
750 48 h in an anaerobic chamber, and continued incubation for 10 d. Surviving bacteria were
751 enumerated on 7H10 agar. The error bars represent the standard derivation of three biological
752 replicates. The experiment was repeated twice with similar results.
753
754 **Figure 4. Inhibition of DosR DNA-binding by HC104A.** (**a**) DosR protein ranging from 0.5 μM
755 to 4 μM was treated with DMSO or 40 μM HC104A and binding to the *hspX* promoter was
756 examined by EMSA. HC104A inhibits DosR DNA binding at 2 μM concentration. (**b**) The free
757 DNA of each reaction was quantified in ImageJ and the percentage of free DNA was normalized
758 using reactions containing 0.5 μM DosR as 100% free DNA. Differences between reactions
759 containing 2 μM DosR treated with DMSO or HC104A are significant (***P* value <0.005 based
760 on a *t*-test). The error bars represent the standard derivation of two biological replicates. (**c**)
761 Dose-dependent impact of HC104A on DosR DNA binding. DosR protein at 2 μM was treated
762 with HC104A at concentrations from 1 μM to 80 μM. (**c**) The free DNA of each reaction was also
763 quantified in ImageJ with the percentage of free DNA is normalized using the reaction
764 containing 80 μM HC104A as 100% free DNA. The differences between treated reactions as
765 compared to DMSO control are significant. (**P* value <0.05 and ***P* value <0.005 based on a *t*-
766 test). The error bars represent the standard derivation of two biological reps.
767

768 **Figure 5. Interactions between HC106A and DosS heme.** WT DosS protein was treated with
769 dithionite (DTN) and then 100 μM HC106A (**a**) or 100 μM pf CORM-2 (a CO donor) (**b**). The UV-
770 visible spectra of the two treatments exhibited a shift of the Soret peak to a common position of
771 422 nm. (**c**) DosS with a G117L amino acid substitution, that is predicted to block the heme
772 exposing channel, provides resistance to HC106A. The spectrum of the mutant protein did not
773 change, after HC106A treatment, indicating resistance to HC106A. (**d**) Overexpression of DosS
774 protein promotes resistance to HC106A treatment in Mtb. Mtb cells with the pVV16 empty vector
775 or the DosS overexpression plasmid were treated with 20 μM HC106A for 6 d. Bacterial RNA
776 was isolated for analysis of the differential gene expression of *hspX* and *tgs1* and analyzed by
777 qRT-PCR. Overexpression of DosS caused 23- and 16.5-fold increase of *hspX* and *tgs1*
778 transcripts, respectively, compared to the empty vector control (****P* value <0.0001 based on a
779 *t*-test). The error bar represents the standard derivation of the mean for three technical
780 replicates. The experiments were repeated twice with a similar result.
781
782 **Figure 6. Synergistic interactions between DosRST inhibitors.** CDC1551 (*hspX'::GFP*) was
783 treated with pairwise combinations of two compounds at concentrations of 50 μM to 0.08 μM.
784 GFP fluorescence was measured and used to calculate percentage inhibition. The data were
785 analyzed in the CompuSyn software to determine the combination index (CI) for the panel of
786 each drug combination, including (**a**) artemisinin and HC102A; (**b**) artemisinin and HC103A; (**c**)
787 artemisinin and HC104A; and (**d**) artemisinin and HC106A. Example EC_{50} curves are presented
788 with individual compounds or a selected synergistic combination to illustrate the potentiating
789 interactions.
790
791 **Table 1. Initial SAR studies of the HC106 series. The HC106 analogs with different R-**
792 **groups were synthesized or purchased. The reporter strain CDC1551 (*hspX'::GFP*) was**

793 **treated with across doses of each analog from 200 μM to 0.328 μM. The EC_{50} values of**

794 **fluorescence inhibition calculated for each analog to determine their potency.**

795

796 **Table 2. Early SAR studies of "A-ring" analogs of HC106.** The HC106 analogs with different

797 R-groups were synthesized. The reporter strain CDC1551 (*hspX'::GFP*) was treated with across

798 doses of each analog from 200 μM to 0.328 μM. The EC_{50} values of fluorescence inhibition

799 were calculated for each analog to determine their potency. The other chemical properties of the

800 analogs are also included. Kinetic solubility and mouse microsomal stability were both

801 experimentally determined.

802

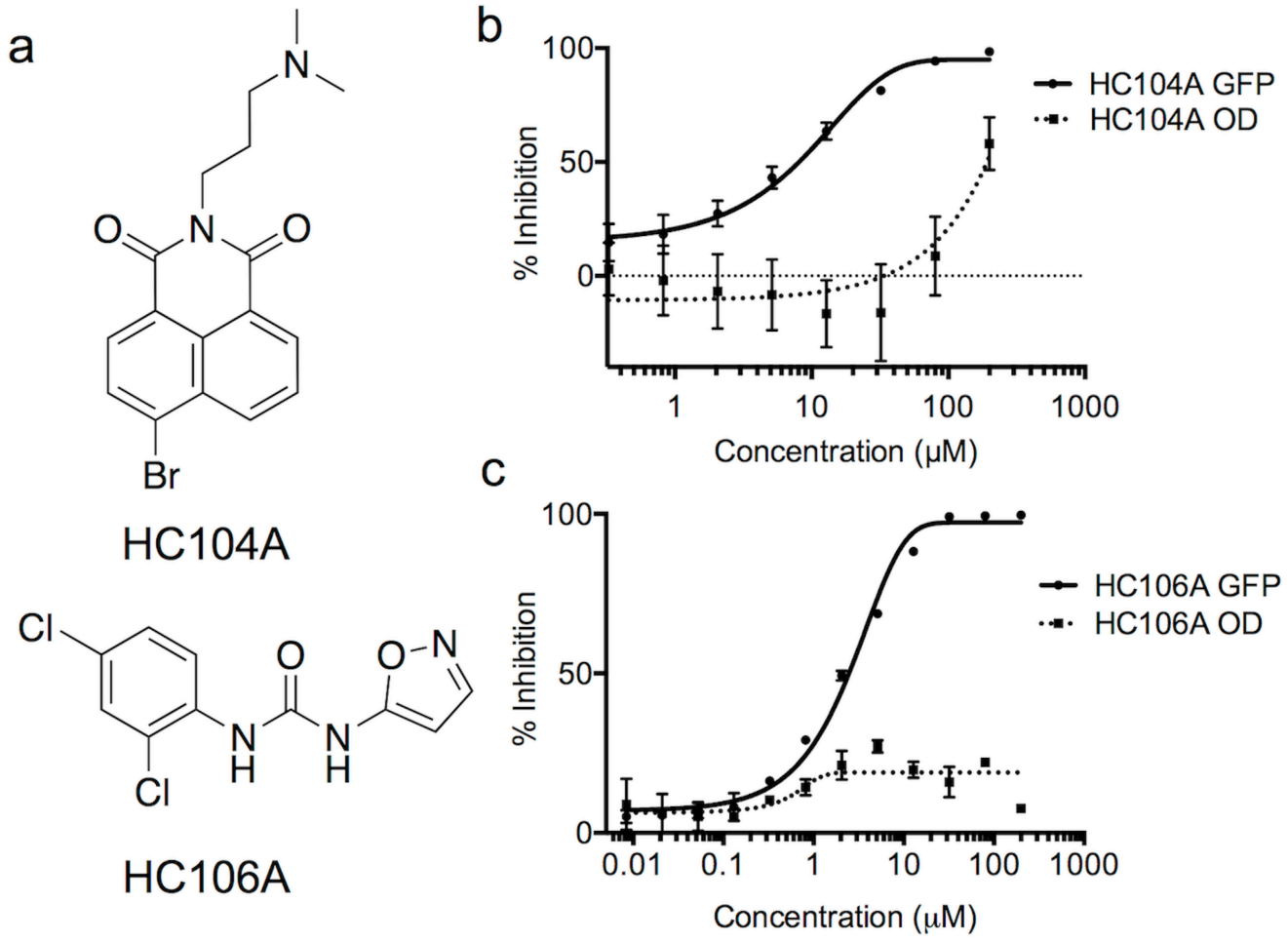
a
N
O
N
O
Br
HC104A
Cl
O
O
N
N
H
N
H
Cl
HC106A
b
100
50
0
% Inhibition
1
10
100
1000
Concentration (μM)
HC104A GFP
HC104A OD
c
100
50
0
% Inhibition
0.01
0.1
1
10
100
1000
Concentration (μM)
HC106A GFP
HC106A OD

Figure 1

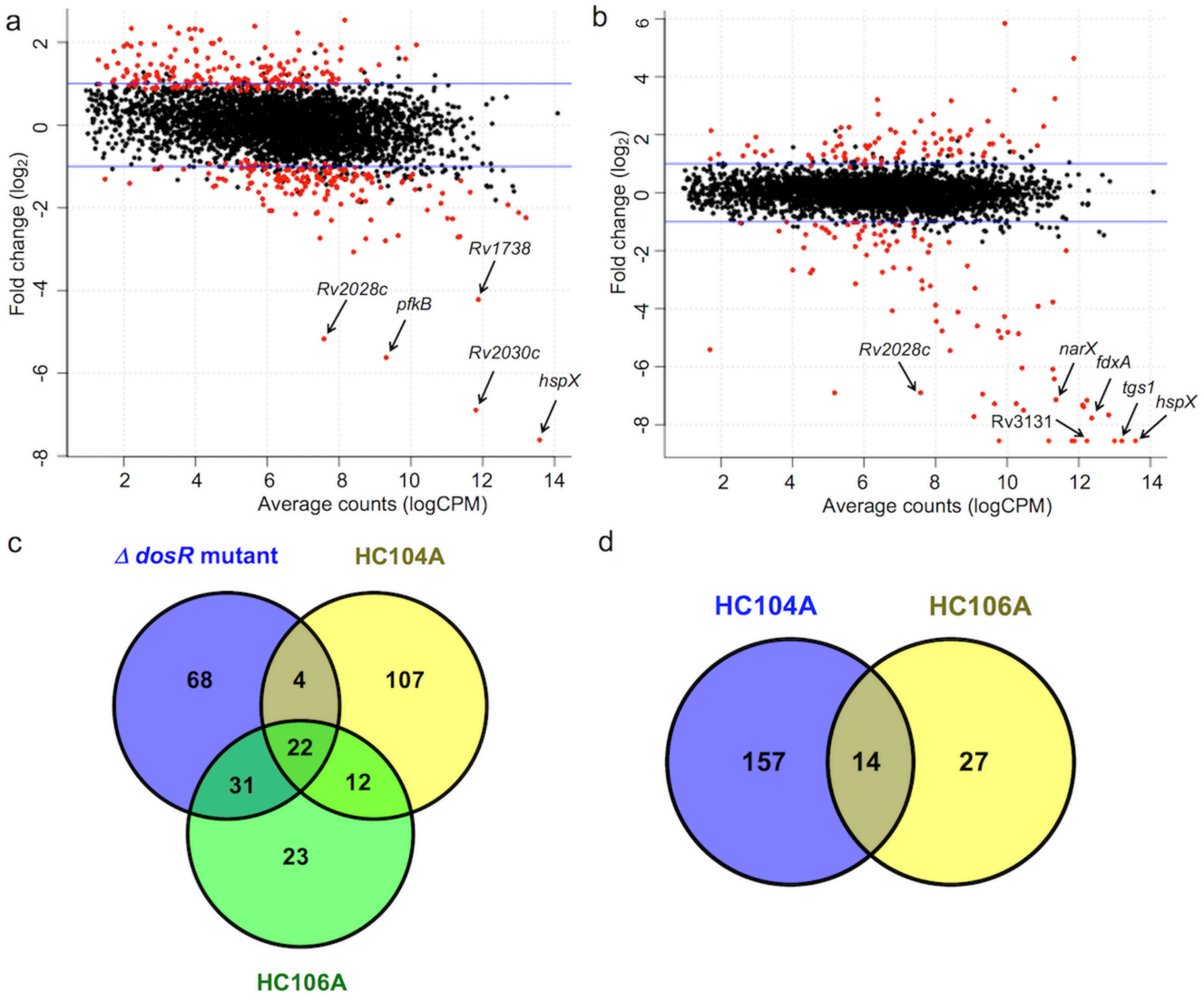
a
Fold change (log2)
Average counts (logCPM)
Rv1738
Rv2028c
pfkB
Rv2030c
hspX
b
Fold change (log2)
Average counts (logCPM)
Rv2028c
narX
fdxA
tgs1
hspX
Rv3131
c
Δ dosR mutant
HC104A
HC106A
68
4
107
22
31
12
23
d
HC104A
HC106A
157
14
27

Figure 2

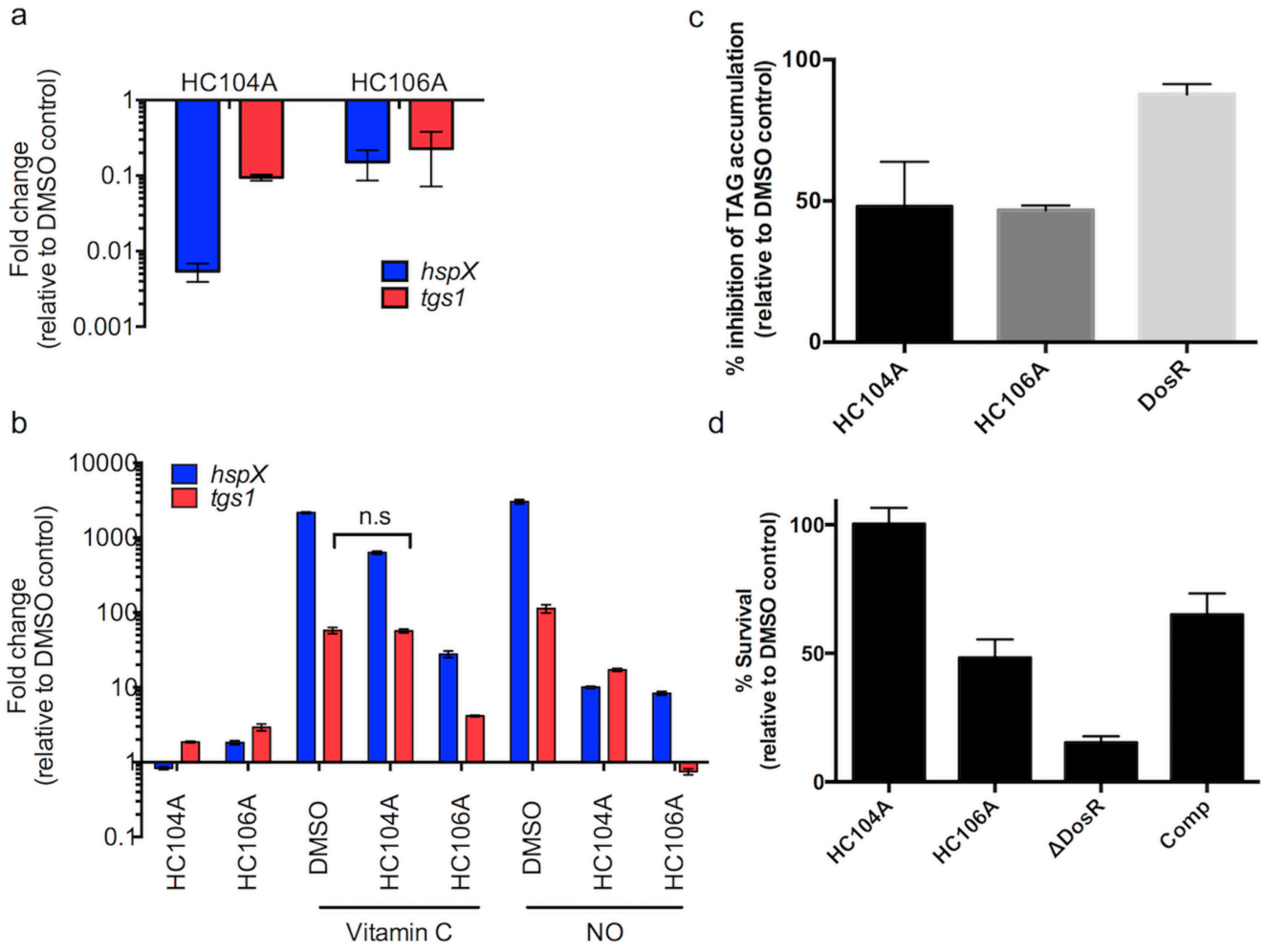
a
HC104A
HC106A
Fold change
(relative to DMSO control)
1
0.1
0.01
0.001
hspX
tgs1
b
10000
1000
100
10
1
0.1
hspX
tgs1
n.s
Fold change
(relative to DMSO control)
HC104A
HC106A
DMSO
HC104A
HC106A
DMSO
HC104A
HC106A
Vitamin C
NO
c
% inhibition of TAG accumulation
(relative to DMSO control)
100
50
0
HC104A
HC106A
DosR
d
% Survival
(relative to DMSO control)
100
50
0
HC104A
HC106A
ΔDosR
Comp

Figure 3

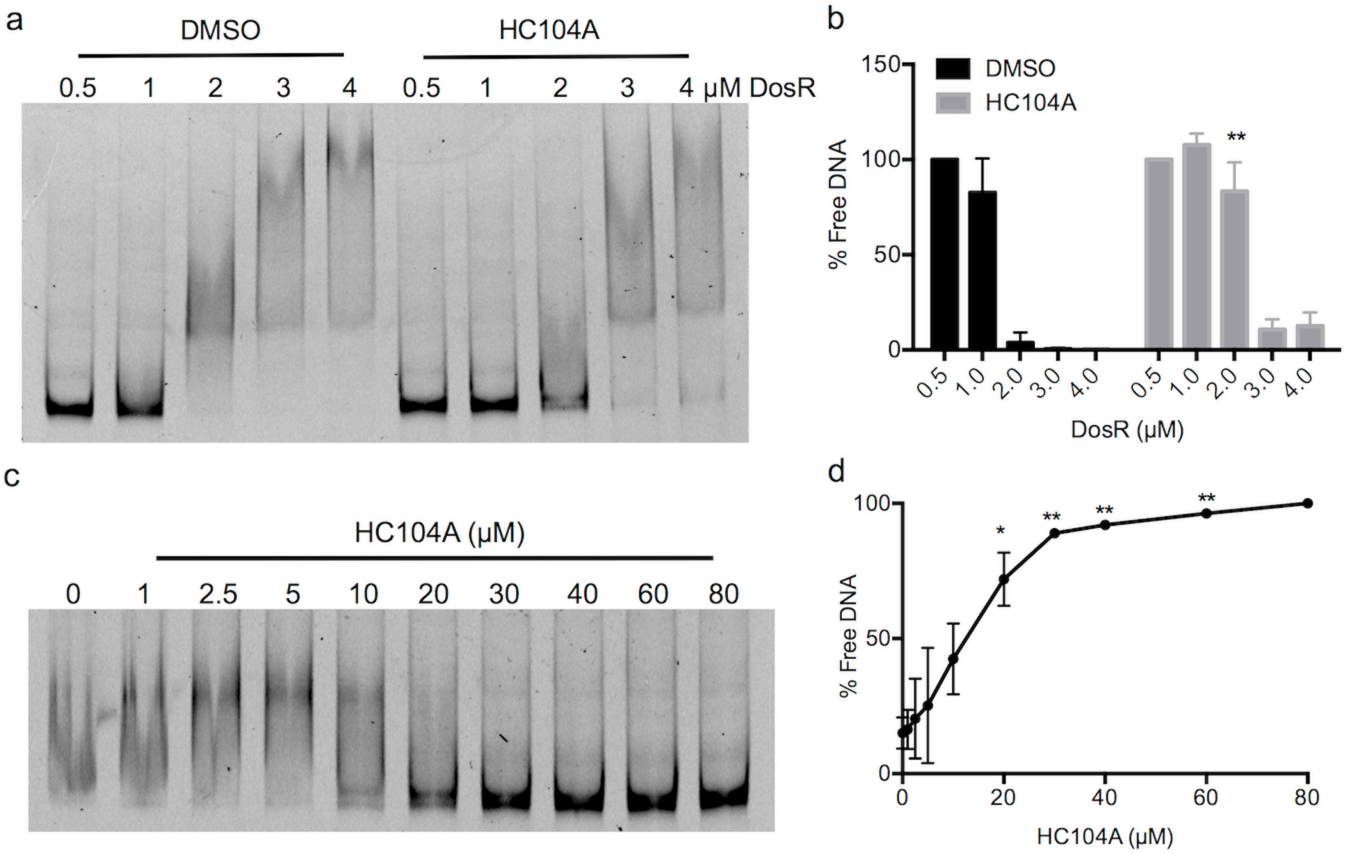
a
DMSO
HC104A
0.5 1 2 3 4 0.5 1 2 3 4 μM DosR
b
DMSO
HC104A
% Free DNA
150
100
50
0
**
0.5 1.0 2.0 3.0 4.0 0.5 1.0 2.0 3.0 4.0
DosR (μM)
c
HC104A (μM)
0 1 2.5 5 10 20 30 40 60 80
d
% Free DNA
100
50
0
*
**
**
**
0 20 40 60 80
HC104A (μM)

Figure 4

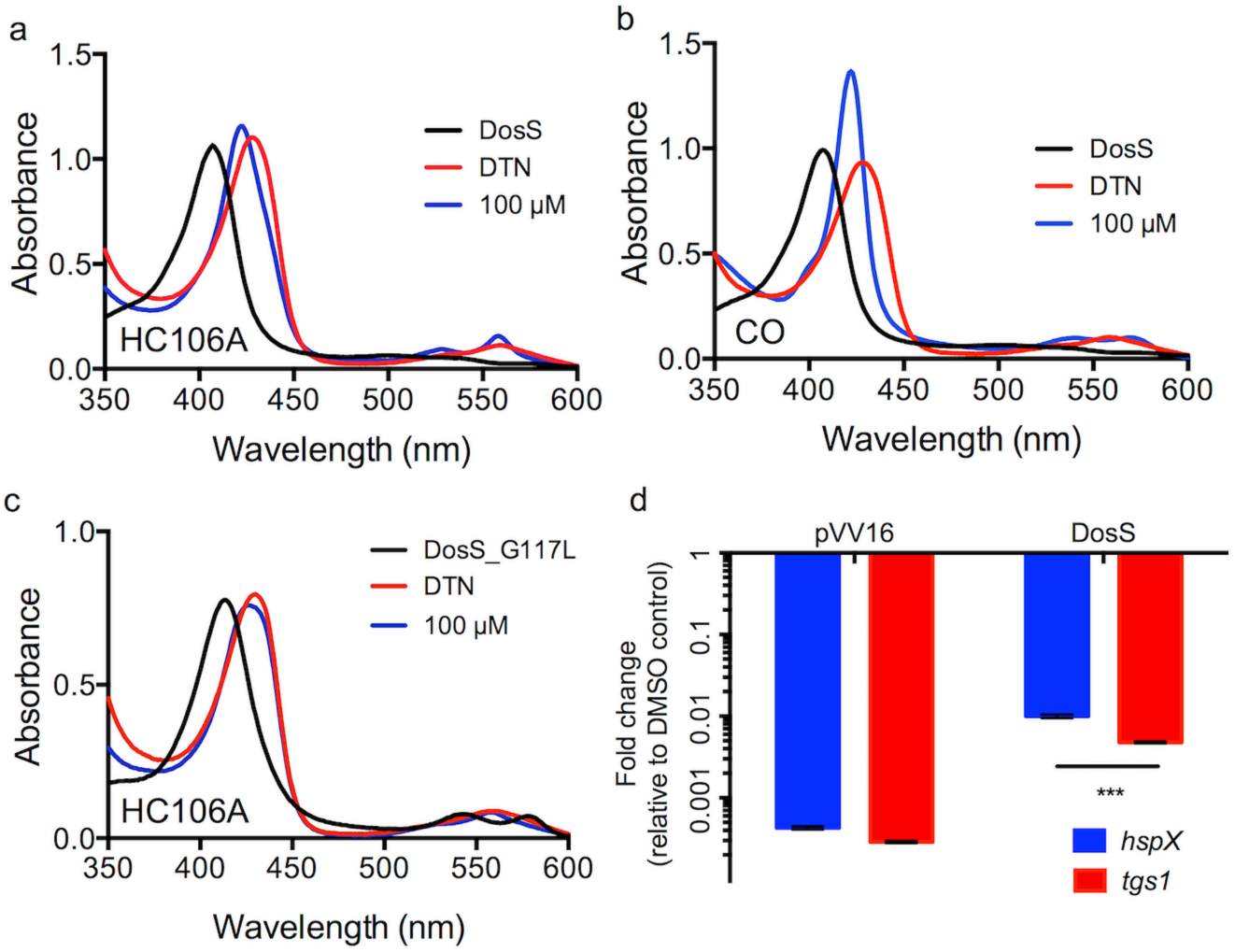
a
Absorbance
1.5
1.0
0.5
0.0
HC106A
DosS
DTN
100 μM
350
400
450
500
550
600
Wavelength (nm)
b
Absorbance
1.5
1.0
0.5
0.0
CO
DosS
DTN
100 μM
350
400
450
500
550
600
Wavelength (nm)
c
Absorbance
1.0
0.5
0.0
HC106A
DosS_G117L
DTN
100 μM
350
400
450
500
550
600
Wavelength (nm)
d
pVV16
DosS
Fold change
(relative to DMSO control)
1
0.1
0.01
0.001
***
hspX
tgs1

Figure 5

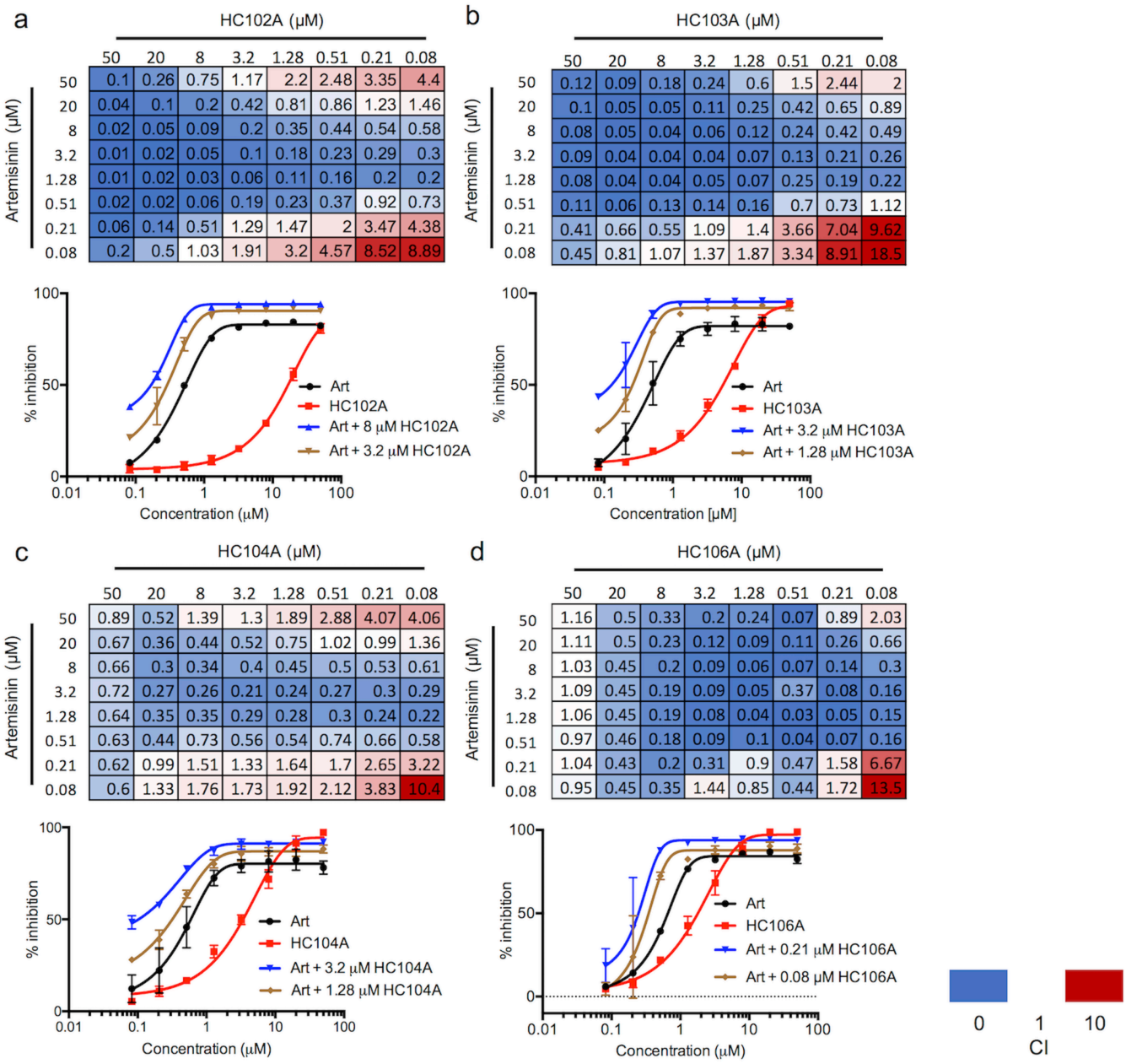
a
HC102A (μM)
50 20 8 3.2 1.28 0.51 0.21 0.08
Artemisinin (μM)
50 0.1 0.26 0.75 1.17 2.2 2.48 3.35 4.4
20 0.04 0.1 0.2 0.42 0.81 0.86 1.23 1.46
8 0.02 0.05 0.09 0.2 0.35 0.44 0.54 0.58
3.2 0.01 0.02 0.05 0.1 0.18 0.23 0.29 0.3
1.28 0.01 0.02 0.03 0.06 0.11 0.16 0.2 0.2
0.51 0.02 0.02 0.06 0.19 0.23 0.37 0.92 0.73
0.21 0.06 0.14 0.51 1.29 1.47 2 3.47 4.38
0.08 0.2 0.5 1.03 1.91 3.2 4.57 8.52 8.89
% inhibition
Concentration (μM)
Art
HC102A
Art + 8 μM HC102A
Art + 3.2 μM HC102A
b
HC103A (μM)
50 20 8 3.2 1.28 0.51 0.21 0.08
Artemisinin (μM)
50 0.12 0.09 0.18 0.24 0.6 1.5 2.44 2
20 0.1 0.05 0.05 0.11 0.25 0.42 0.65 0.89
8 0.08 0.05 0.04 0.06 0.12 0.24 0.42 0.49
3.2 0.09 0.04 0.04 0.04 0.07 0.13 0.21 0.26
1.28 0.08 0.04 0.04 0.05 0.07 0.25 0.19 0.22
0.51 0.11 0.06 0.13 0.14 0.16 0.7 0.73 1.12
0.21 0.41 0.66 0.55 1.09 1.4 3.66 7.04 9.62
0.08 0.45 0.81 1.07 1.37 1.87 3.34 8.91 18.5
% inhibition
Concentration [μM]
Art
HC103A
Art + 3.2 μM HC103A
Art + 1.28 μM HC103A
c
HC104A (μM)
50 20 8 3.2 1.28 0.51 0.21 0.08
Artemisinin (μM)
50 0.89 0.52 1.39 1.3 1.89 2.88 4.07 4.06
20 0.67 0.36 0.44 0.52 0.75 1.02 0.99 1.36
8 0.66 0.3 0.34 0.4 0.45 0.5 0.53 0.61
3.2 0.72 0.27 0.26 0.21 0.24 0.27 0.3 0.29
1.28 0.64 0.35 0.35 0.29 0.28 0.3 0.24 0.22
0.51 0.63 0.44 0.73 0.56 0.54 0.74 0.66 0.58
0.21 0.62 0.99 1.51 1.33 1.64 1.7 2.65 3.22
0.08 0.6 1.33 1.76 1.73 1.92 2.12 3.83 10.4
% inhibition
Concentration (μM)
Art
HC104A
Art + 3.2 μM HC104A
Art + 1.28 μM HC104A
d
HC106A (μM)
50 20 8 3.2 1.28 0.51 0.21 0.08
Artemisinin (μM)
50 1.16 0.5 0.33 0.2 0.24 0.07 0.89 2.03
20 1.11 0.5 0.23 0.12 0.09 0.11 0.26 0.66
8 1.03 0.45 0.2 0.09 0.06 0.07 0.14 0.3
3.2 1.09 0.45 0.19 0.09 0.05 0.37 0.08 0.16
1.28 1.06 0.45 0.19 0.08 0.04 0.03 0.05 0.15
0.51 0.97 0.46 0.18 0.09 0.1 0.04 0.07 0.16
0.21 1.04 0.43 0.2 0.31 0.9 0.47 1.58 6.67
0.08 0.95 0.45 0.35 1.44 0.85 0.44 1.72 13.5
% inhibition
Concentration (μM)
Art
HC106A
Art + 0.21 μM HC106A
Art + 0.08 μM HC106A
0 1 10
CI

Figure 6

ID#	Compound	EC_{50} (μM)	ID#	Compound	EC_{50} (μM)
HC106F	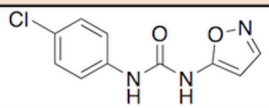	1.33	MSU-41324	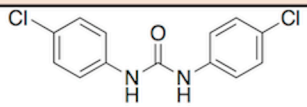	>200
HC106A	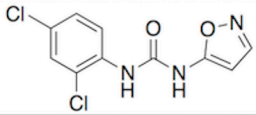	2.48	MSU-39449	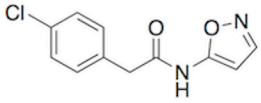	5.2
HC106C	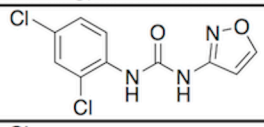	>200	MSU-39451	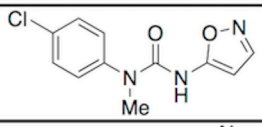	4.14
MSU-39450	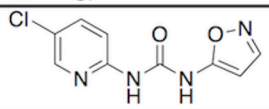	1.95	MSU-39453	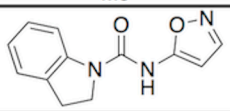	16.62
MSU-39444	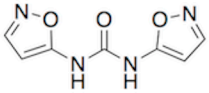	1.7	MSU-41422	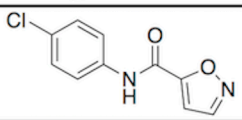	>200
MSU-41425	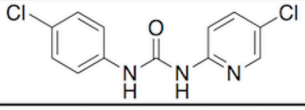	>200			

Table 1

	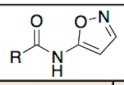								
ID#	Compound R =	EC_{50} (μM)	MW (g/mol)	TPSA (ang^2)	Ligand Efficiency (LE)	m.p. (°C)	cLogP	Solubility (μM)	Microsomes (% remaining @ 30 minutes)
HC106F	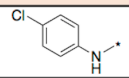	1.33	237.6	63	0.50	183	2.2	>200	115%
HC106A	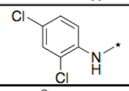	2.48	272.1	63	0.41	164	2.7	110	-
MSU-33189		0.63	203.1	63	0.56	183-184	1.6	-	-
MSU-39447	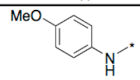	0.61	233.2	72	0.49	166-167	1.5	>100	-
MSU-39448	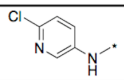	1.42	238.6	75	0.49	158-159	1.3	-	-
MSU-39450	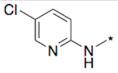	1.95	238.6	75	0.38	122-123	1.3	-	-
MSU-39446	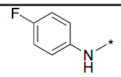	0.54	221.2	63	0.52	176-177	1.7	>100	70%
MSU-41464	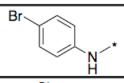	1.2	282.1	67	0.51	183-184	2.3	-	109%
MSU-39445	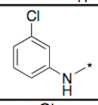	0.75	237.6	63	0.52	159 (dec)	2.1	>100	-
MSU-39452	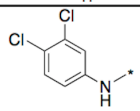	2.47	272.1	63	0.45	164	2.8	-	-
MSU-41442	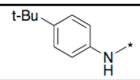	2.08	259.3	63	0.41	163	3.1	>100	-
MSU-41443	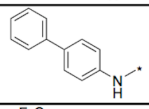	11.2	279.3	63	0.32	193	3.2	14	-
MSU-41463	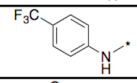	1.67	271.2	67	0.42	178	2.4	-	84
MSU-41465	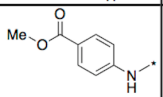	1.16	261.2	94	0.43	194	1.5	-	73
MSU-41462	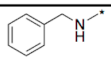	1.12	217.2	67	0.45	128-130	1.3	-	-
MSU-41542	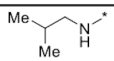	1.34	183.2	67	0.62	187	0.9	-	-
MSU-41545	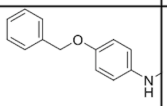	4.75	309.3	76	0.32	164	2.9	-	-
MSU-41546		2.15	195.2	67	0.56	182	1.1	-	-
MSU-42002		1.21	209.2	67	0.54	180	1.4	-	-
MSU-42003	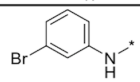	1.94	282.1	67	0.49	157	2.3	-	-
MSU-42004	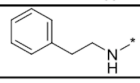	2.36	231.3	67	0.45	165	1.7	-	-

Table 2

Supplementary Methods and Figures

Inhibition of *Mycobacterium tuberculosis* DosRST two-component regulatory system signaling by targeting response regulator DNA binding and sensor kinase heme

Huiqing Zheng[*], Bilal Aleiwi[†], Edmund Ellsworth[†], and Robert B. Abramovitch[*‡]

[1]Department of Microbiology and Molecular Genetics, [2]Department of Pharmacology and Toxicology, Michigan State University, East Lansing, Michigan, 48824

Supplemental Methods

Experimental procedures for urea formation

Formation of acyl chloride **2**. To a stirred solution of isoxazole acid **1** (1 eq.) in dry tetrahydrofuran (THF, 0.4 M) under N_2 atmosphere was added oxalyl chloride (1.5 eq.) dropwise over 5-10 min followed by dimethylformamide (DMF) (cat.) and the reaction mixture was continued to stir at room temperature. Upon completion, the reaction mixture was concentrated into a residue in *vacuo* and the residue was dissolved in THF and concentrated again to ensure the removal of excess oxalyl chloride. The crude acyl chloride **2** was used directly in the next step without further purification.

Formation of acyl azide and rearrangement into isocyanate **3**.

The crude acyl chloride **2** was dissolved in THF (0.4 M) and stirred at room temperature under N_2 atmosphere. Trimethylsilyl (TMS) azide (2 eq.) was added dropwise over 5 min and stirring was continued. Upon completion of the reaction, the mixture was diluted with ethyl acetate (0.4 M) and quenched with H_2O (0.4 M). The two layers were separated, and the organic layer was dried over anhydrous Na_2SO_4 and filtered. The ethyl acetate solvent was swapped into toluene (0.1 M) by the addition of toluene followed by removal of the ethyl acetate in *vacuo*. Care was taken not to concentrate the toluene. The toluene acyl azide solution was heated at reflux conditions under N_2 atmosphere for 4 h to give the desired isocyanate **3** which was used as a solution in toluene in the next step.

Formation of urea **4**. The crude isocyanate solution in toluene was mixed with different amines (1.5 eq.) and stirred at room temperature overnight. Isolation of the ureas was done by diluting the reaction mixture with hexanes, stirring for few hours and filtration of the formed precipitate. The solid material was washed with hexanes and dried under high vacuum. The urea products usually do not require further purifications. All products were analyzed by ^{1}H NMR and high-resolution mass spectrometry (HRMS).

Synthesis of ***MSU-41422*** (amide) from acyl chloride **2**. Acyl chloride **2** (1 eq.) was dissolved in dichloromethane (DCM, 0.2 M) and 4-chloroaniline (1.2 eq.) was added. The reaction mixture was stirred at room temperature overnight. The reaction mixture was concentrated in *vacuo* and the residue was purified by flash column chromatography.

Synthesis of ***MSU-39449***. A slurry of 4-chlorophenyl acetic acid (0.10 g, 0.60 mmoles) in 2.0 mL of DCM was treated with oxalyl chloride (0.12 mL, 0.9 mmoles) and 1 drop of DMF. The mixture (with gas evolution) gradually became homogeneous and was stirred for 30 min. The mixture was concentrated in *vacuo*, diluted with 5 mL of DCM and again concentrated in vacuo, the process repeated three times. The resulting residue was again dissolved in DCM (2 mL) and treated with 5-aminoisoxazole (0.030 g., 0.36 mmoles), followed by pyridine (0.48 mL, 0.6 mmoles). The mixture was then allowed to stir overnight. The mixture was then quenched with 1.0 N HCl and extracted with DCM. The organic layers were combined, washed with saturated $KHCO_3$, dried with Na_2SO_4 and concentrated in *vacuo*. Medium pressure liquid chromatography (SiO_2, 100% DCM to 3% methanol / DCM) to provide a solid (0.023 g).

^{1}H NMR and HRMS data:

MSU# 39444. ^{1}H NMR (500 MHz, DMSO-d_6) δ 10.54 (s, 2H), 8.44 (d, J = 1.9 Hz, 2H), 6.11 (d, J = 2.0 Hz, 2H). HRMS (ESI) m/z calculated for $C_7H_6N_4O_3$ [M+H], 195.0513 found 195.0518.

MSU# 39449. ^{1}H NMR (500 MHz, DMSO-d_6) δ 11.91 (s, 1H), 8.41 (s, 1H), 7.39 (d, J = 2.0 Hz, 2H), 7.35 (d, J = 2.0 Hz, 2H), 6.19 (s, 1H), 3.73 (s, 2H). HRMS (ESI) m/z calculated for $C_{11}H_{10}ClN_2O_2$ [M-H], 235.0269; found 235.1989.

MSU# 39445. ^{1}H NMR (500 MHz, DMSO-d_6) δ 10.41 (s, 1H), 9.14 (s, 1H), 8.40 (d, J = 2.0 Hz, 1H), 7.82 – 7.58 (m, 1H), 7.31 (dd, J = 4.9, 1.8 Hz, 2H), 7.07 (dt, J = 6.4, 2.3 Hz, 1H), 6.06 (d, J = 1.9 Hz, 1H). HRMS (ESI) m/z calculated for $C_{10}H_9ClN_3O_2$ [M+H], 238.0378; found 238.0365.

MSU# 39452. ^{1}H NMR (500 MHz, DMSO-d_6) δ 10.50 (s, 1H), 9.23 (s, 1H), 8.51 – 8.28 (m, 1H), 7.86 (d, *J* = 2.5 Hz, 1H), 7.64 – 7.43 (m, 1H), 7.37 (dd, *J* = 8.9, 2.5 Hz, 1H), 6.26 – 5.80 (m, 1H). HRMS (ESI) m/z calculated for $C_{10}H_8Cl_2N_3O_2$ [M+H], 271.9989; found 271.9969.

MSU# 39447. ^{1}H NMR (500 MHz, DMSO-d6) δ 8.83 (s, 1H), 8.43 – 8.29 (m, 1H), 7.36 (d, *J* = 8.4 Hz, 2H), 6.86 (d, *J* = 8.6 Hz, 2H), 6.00 (d, *J* = 1.9 Hz, 1H), 3.70 (s, 3H). HRMS (ESI) m/z calculated for $C_{11}H_{12}N_3O_3$ [M+H], 234.0874; found 234.0863.

MSU# 39451. ^{1}H NMR (500 MHz, DMSO-d6) δ 10.13 (s, 1H), 8.34 (d, *J* = 1.9 Hz, 1H), 7.56 – 7.41 (m, 2H), 7.41 – 7.22 (m, 2H), 6.04 (d, *J* = 2.0 Hz, 1H), 3.25 (s, 3H). HRMS (ESI) m/z calculated for $C_{11}H_{11}ClN_3O_2$ [M+H], 252.0535; found 252.0596.

MSU# 39453. ^{1}H NMR (500 MHz, DMSO-d6) δ 10.49 (s, 1H), 8.41 (d, *J* = 1.9 Hz, 1H), 7.84 (d, *J* = 8.7 Hz, 1H), 7.27 (dt, *J* = 2.3, 1.1 Hz, 1H), 7.18 (dt, *J* = 8.8, 1.6 Hz, 1H), 6.14 (d, *J* = 1.9 Hz, 1H), 4.13 (dd, *J* = 9.1, 8.2 Hz, 2H), 3.17 (t, *J* = 8.6 Hz, 2H). HRMS (ESI) m/z calculated for $C_{12}H_{11}ClN_3O_2$ [M+H], 264.0535; found 264.0552.

MSU# 39448. ^{1}H NMR (500 MHz, DMSO-d6) δ 10.55 (s, 1H), 9.25 (s, 1H), 8.64 – 8.24 (m, 2H), 7.98 (d, *J* = 8.6 Hz, 1H), 7.45 (d, *J* = 8.6 Hz, 1H), 6.08 (d, *J* = 18.1 Hz, 1H). HRMS (ESI) m/z calculated for $C_9H_8ClN_4O_2$ [M+H], 239.0331; found 239.0364.

MSU# 39450. ^{1}H NMR (500 MHz, DMSO-d6) δ 11.00 (s, 1H), 9.66 (s, 1H), 8.42 (d, *J* = 1.9 Hz, 1H), 8.34 (d, *J* = 2.6 Hz, 1H), 7.96 – 7.79 (m, 1H), 7.73 (d, *J* = 8.9 Hz, 1H), 6.10 (q, *J* = 2.7, 2.2 Hz, 2H). HRMS (ESI) m/z calculated for $C_9H_8ClN_4O_2$ [M+H], 239.0331; found 239.0356.

MSU# 39446. ^{1}H NMR (500 MHz, DMSO-d_6) δ 10.24 (s, 1H), 8.90 (s, 1H), 8.38 (d, *J* = 1.9 Hz, 1H), 7.54 – 7.37 (m, 2H), 7.26 – 7.02 (m, 2H), 6.03 (d, *J* = 2.0 Hz, 1H). HRMS (ESI) m/z calculated for $C_{10}H_9FN_3O_2$ [M+H], 222.0674; found 222.0675.

MSU# 41422. ^{1}H NMR (500 MHz, Chloroform-d) δ 8.41 (d, *J* = 1.8 Hz, 1H), 8.26 (s, 1H), 7.71 – 7.52 (m, 2H), 7.44 – 7.33 (m, 2H), 7.06 (d, *J* = 1.8 Hz, 1H). HRMS (ESI) m/z calculated for $C_{10}H_8ClN_2O_2$ [M+H], 223.0269; found 223.0265.

MSU# 41324. ^{1}H NMR (500 MHz, DMSO-d6) δ 9.91 (s, 1H), 9.50 (s, 1H), 8.31 (d, *J* = 2.6 Hz, 1H), 7.85 (dd, *J* = 9.0, 2.7 Hz, 1H), 7.67 (d, *J* = 8.9 Hz, 1H), 7.39 – 7.30 (m, 2H). HRMS (ESI) m/z calculated for $C_{12}H_{10}Cl_2N_3O$ [M+H], 282.0196; found 282.0182.

MSU# 41425. ^{1}H NMR (500 MHz, DMSO-d_6) δ 8.83 (s, 1H), 7.53 – 7.39 (m, 2H), 7.39 – 7.16 (m, 2H). HRMS (ESI) m/z calculated for $C_{13}H_{11}Cl_2N_2O$ [M+H], 281.0243; found 281.0258.

MSU# 41443. ^{1}H NMR (500 MHz, DMSO-d_6) δ 10.36 (d, *J* = 28.4 Hz, 1H), 9.13 (d, *J* = 45.7 Hz, 1H), 8.40 (d, *J* = 1.9 Hz, 1H), 7.70 – 7.59 (m, 5H), 7.59 – 7.49 (m, 3H), 7.43 (t, *J* = 7.7 Hz, 3H), 7.32 (t, *J* = 7.4 Hz, 1H), 6.06 (d, *J* = 1.9 Hz, 1H). HRMS (ESI) m/z calculated for $C_{16}H_{14}N_3O_2$ [M+H], 280.1081; found 280.1083.

MSU# 41442. ^{1}H NMR (500 MHz, DMSO-d6) δ 10.15 (s, 1H), 8.77 (s, 1H), 8.38 (d, *J* = 1.9 Hz, 1H), 7.44 – 7.27 (m, 4H), 6.03 (d, *J* = 2.0 Hz, 1H), 1.25 (s, 9H). HRMS (ESI) m/z calculated for $C_{14}H_{18}N_3O_2$ [M+H], 260.1394; found 260.1406.

MSU# 33189. ^{1}H NMR (500 MHz, DMSO-d_6) δ 10.20 (s, 1H), 8.85 (s, 1H), 8.39 (d, *J* = 1.9 Hz, 1H), 7.54 – 7.37 (m, 2H), 7.35 – 7.21 (m, 2H), 7.02 (t, *J* = 7.4 Hz, 1H), 6.04 (d, *J* = 1.9 Hz, 1H). HRMS (ESI) m/z calculated for $C_{10}H_{10}N_3O_2$ [M+H], 204.0768; found 204.0777.

MSU# 33231. ^{1}H NMR (500 MHz, DMSO-d6) δ 10.29 (s, 1H), 9.01 (s, 1H), 8.39 (d, *J* = 1.9 Hz, 1H), 7.56 – 7.41 (m, 2H), 7.41 – 7.27 (m, 2H), 6.05 (d, *J* = 1.9 Hz, 1H). HRMS (ESI) m/z calculated for $C_{10}H_9ClN_3O_2$ [M+H], 238.0378; found 238.0391.

MSU# 41462. ^{1}H NMR (500 MHz, DMSO-d_6) δ 10.18 (s, 1H), 8.31 (d, *J* = 2.0 Hz, 1H), 7.43 – 7.07 (m, 3H), 6.92 (s, 1H), 5.94 (d, *J* = 1.9 Hz, 1H), 4.30 (d, *J* = 6.0 Hz, 2H). HRMS (ESI) m/z calculated for $C_{11}H_{12}N_3O_2$ [M+H], 218.0924 found 218.0956.

MSU# 41463. ^{1}H NMR (500 MHz, DMSO-d_6) δ 10.39 (s, 1H), 9.29 (s, 1H), 8.41 (d, *J* = 1.9 Hz, 1H), 7.67 (d, *J* = 1.0 Hz, 4H), 6.08 (d, *J* = 1.9 Hz, 1H). HRMS (ESI) m/z calculated for $C_{11}H_9F_3N_3O_2$ [M+H], 272.0642; found 272.0653.

MSU# 41464. ^{1}H NMR (500 MHz, DMSO-d_6) δ 10.29 (s, 1H), 9.01 (s, 1H), 8.39 (d, *J* = 1.9 Hz, 2H), 7.50 – 7.45 (m, 1H), 7.45 – 7.40 (m, 1H), 6.05 (s, 1H). HRMS (ESI) m/z calculated for $C_{10}H_9BrN_3O_2$ [M+H], 281.9873; found 281.9876.

MSU# 41465. ^{1}H NMR (500 MHz, DMSO-d_6) δ 10.38 (s, 1H), 9.27 (s, 1H), 8.41 (d, *J* = 2.0 Hz, 1H), 8.00 – 7.79 (m, 2H), 7.66 – 7.48 (m, 2H), 6.08 (d, *J* = 1.9 Hz, 1H), 3.81 (s, 3H). HRMS (ESI) m/z calculated for $C_{12}H_{12}N_3O_4$ [M+H], 262.0823; found 262.0827.

MSU# 41545. ^{1}H NMR (500 MHz, DMSO-d_6) δ 10.17 (s, 1H), 8.71 (s, 1H), 8.37 (d, *J* = 1.9 Hz, 1H), 7.57 – 7.14 (m, 5H), 7.11 – 6.69 (m, 2H), 6.02 (d, *J* = 1.9 Hz, 1H), 5.06 (s, 2H).HRMS (ESI) m/z calculated for $C_{17}H_{16}N_3O_3$ [M+H], 310.1187; found 310.1178.

MSU# 41546. ^{1}H NMR (500 MHz, DMSO-d_6) δ 9.69 (s, 1H), 8.30 (d, *J* = 1.9 Hz, 1H), 6.42 (d, *J* = 7.2 Hz, 1H), 5.91 (d, *J* = 1.9 Hz, 1H), 3.92 (h, *J* = 6.7 Hz, 1H), 1.83 (dq, *J* = 12.8, 6.6, 6.0 Hz, 3H), 1.73 – 1.46 (m, 5H), 1.46 – 1.13 (m, 3H). HRMS (ESI) m/z calculated for $C_9H_{14}N_3O_2$ [M+H], 196.1081; found 196.1144.

MSU# 42002. ^{1}H NMR (500 MHz, DMSO-d_6) δ 9.80 (s, 1H), 8.30 (d, *J* = 1.9 Hz, 1H), 6.34 (d, *J* = 7.8 Hz, 1H), 5.90 (d, *J* = 1.9 Hz, 1H), 3.58 – 3.39 (m, 1H), 1.77 (dt, *J* = 11.1, 3.7 Hz, 1H), 1.64 (dt, *J* = 12.9, 4.1 Hz, 1H), 1.52 (dd, *J* = 10.4, 6.3 Hz, 1H), 1.37 – 0.93 (m, 3H). HRMS (ESI) m/z calculated for $C_{10}H_{16}N_3O_2$ [M+H], 210.1238; found 210.1282.

MSU# 42004. ^{1}H NMR (500 MHz, DMSO-d_6) δ 10.07 (s, 2H), 8.31 (d, *J* = 2.0 Hz, 1H), 7.37 – 7.06 (m, 5H), 6.40 (s, 1H), 5.93 (d, *J* = 1.8 Hz, 1H), 3.31 (t, *J* = 7.2 Hz, 2H), 2.74 (t, *J* = 7.2 Hz, 2H). HRMS (ESI) m/z calculated for $C_{12}H_{14}N_3O_2$ [M+H], 232.1081; found 232.1105.

MSU# 42003. ^{1}H NMR (500 MHz, DMSO-d_6) δ 10.36 (s, 1H), 9.06 (s, 1H), 8.40 (d, *J* = 1.9 Hz, 1H), 7.83 (t, *J* = 2.0 Hz, 1H), 7.46 – 7.03 (m, 3H), 6.07 (d, *J* = 2.0 Hz, 1H). HRMS (ESI) m/z calculated for $C_{10}H_9BrN_3O_2$ [M+H], 281.9873; found 281.9915.

MSU# 41542. ^{1}H NMR (500 MHz, DMSO-d_6) δ 10.20 – 9.49 (m, 1H), 8.30 (d, *J* = 1.9 Hz, 1H), 6.44 (t, *J* = 5.9 Hz, 1H), 5.91 (d, *J* = 1.9 Hz, 1H), 2.93 (t, *J* = 6.3 Hz, 2H), 1.68 (dh, *J* = 13.3, 6.7

Hz, 1H), 0.85 (d, *J* = 6.7 Hz, 6H). HRMS (ESI) m/z calculated for $C_8H_{14}N_3O_2$ [M+Na], 206.0899; found 206.0926.

Supplementary Dataset 1. Differential gene expression data of WT Mtb treated with inhibitors

Supplementary Dataset 2. Differential gene expression data of the DosR mutant treated with the inhibitors.

Supplementary Dataset 3. Complete gene expression tables for transcriptional profiling experiments.

Supplemental Table 1 and Figures 1-9

Compound	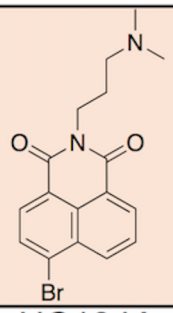	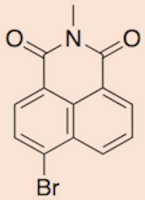	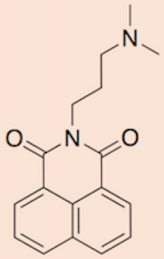
ID#	HC104A	HC104G	HC104B
MW (g/mole)	361.2	290.1	282.3
EC_{50} (μM)	9.8	43.8	>200
Ligand Efficiency	0.34	0.36	0.26
CLogP (cLogD at pH 7.4)	3.0 (0.55)	2.3 (2.4)	2.9 (-0.24)
Druglikeness	4.4	0.55	6.2

Supplemental Table 1. Structure and properties of HC104 series. Catalog structure activity relationship study performed for HC104 analogs with different R-groups. The reporter strain CDC1551 (hspX'::GFP) was treated across doses of each analog from 200 μM to 0.328 μM. The EC50 values of fluorescence inhibition calculated for each analog to determine their potency. The other chemical properties of the analogs are also included.

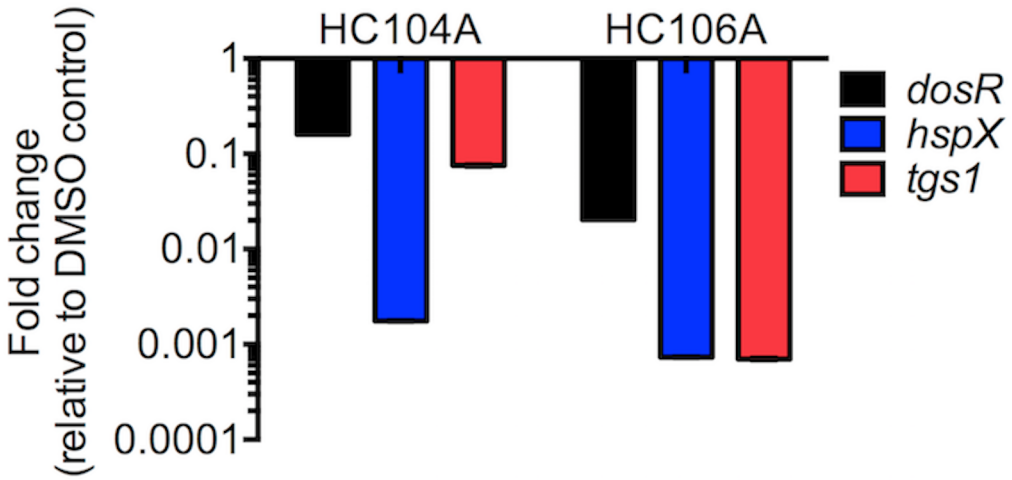

Supplemental Figure 1. Inhibition of the DosR regulon by HC104 and HC106A during hypoxia. Mtb cells were treated with 40 μM compounds for 6 d, and total bacterial RNA was isolated. The DosR regulated genes, dosR, hspX, and tgs1 were quantified in qRT-PCR. The error bars represent the standard derivation of three replicates. The experiment was repeated at least twice with similar results.

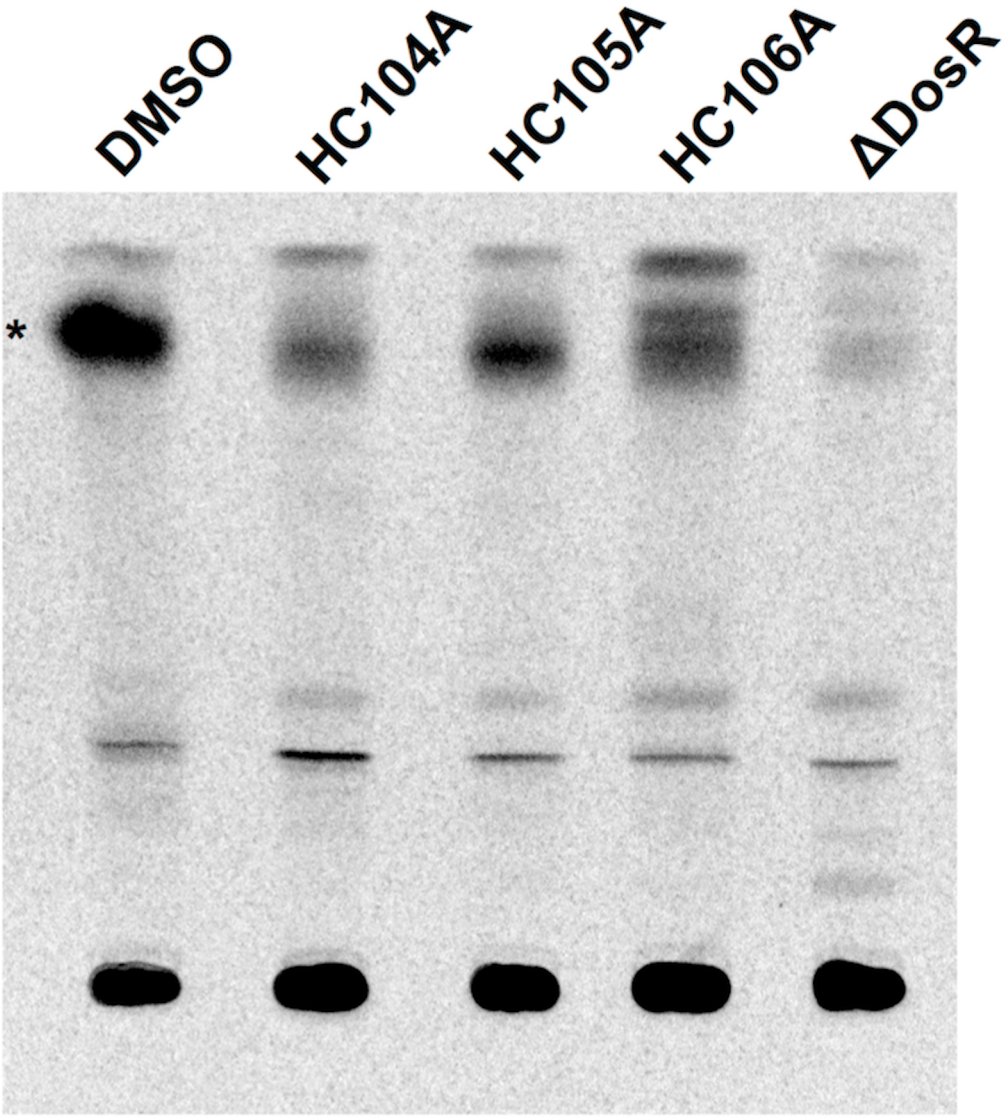

Supplemental Figure 2. TLC of TAG reduction in Mtb treated with HC104A and HC106A. Mtb cells were treated with 40 μM of the compounds and labeled with [1,2-14C] sodium acetate in T25 vented tissue culture flasks for 6 d. Total lipid was isolated and analyzed BY TLC. The experiment was repeated twice with similar results.

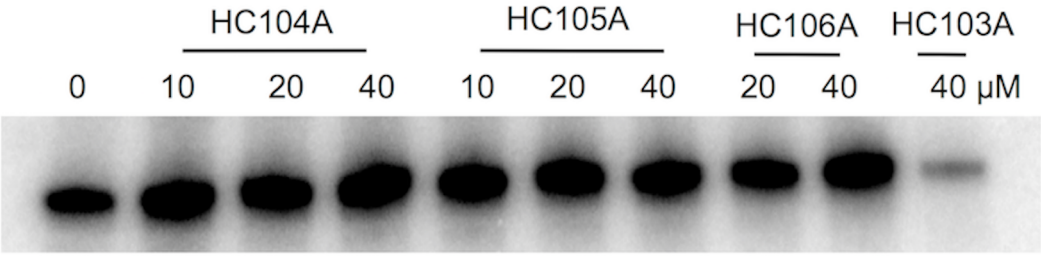

Supplemental Figure 3. Autoradiograph examining the impact of HC104A and HC106A on DosS autophosphorylation. DosS protein was treated with 10 μM, 20 μM or 40 μM of the compounds, with DMSO and HC103A as positive and negative controls, respectively. The results show that HC104A and HC106A have no effect on DosS autophosphorylation.

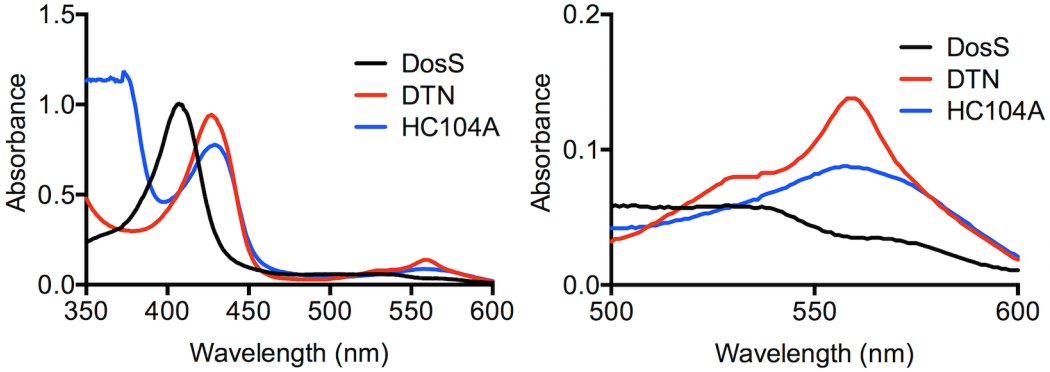

Supplemental Figure 4. Investigation of interaction between HC104A and DosS. WT DosS treated with 400 μM HC104A shows no impact on shifting of the Soret peak in the UV-visible spectroscopy assay. The experiment was repeated at least twice with similar results.

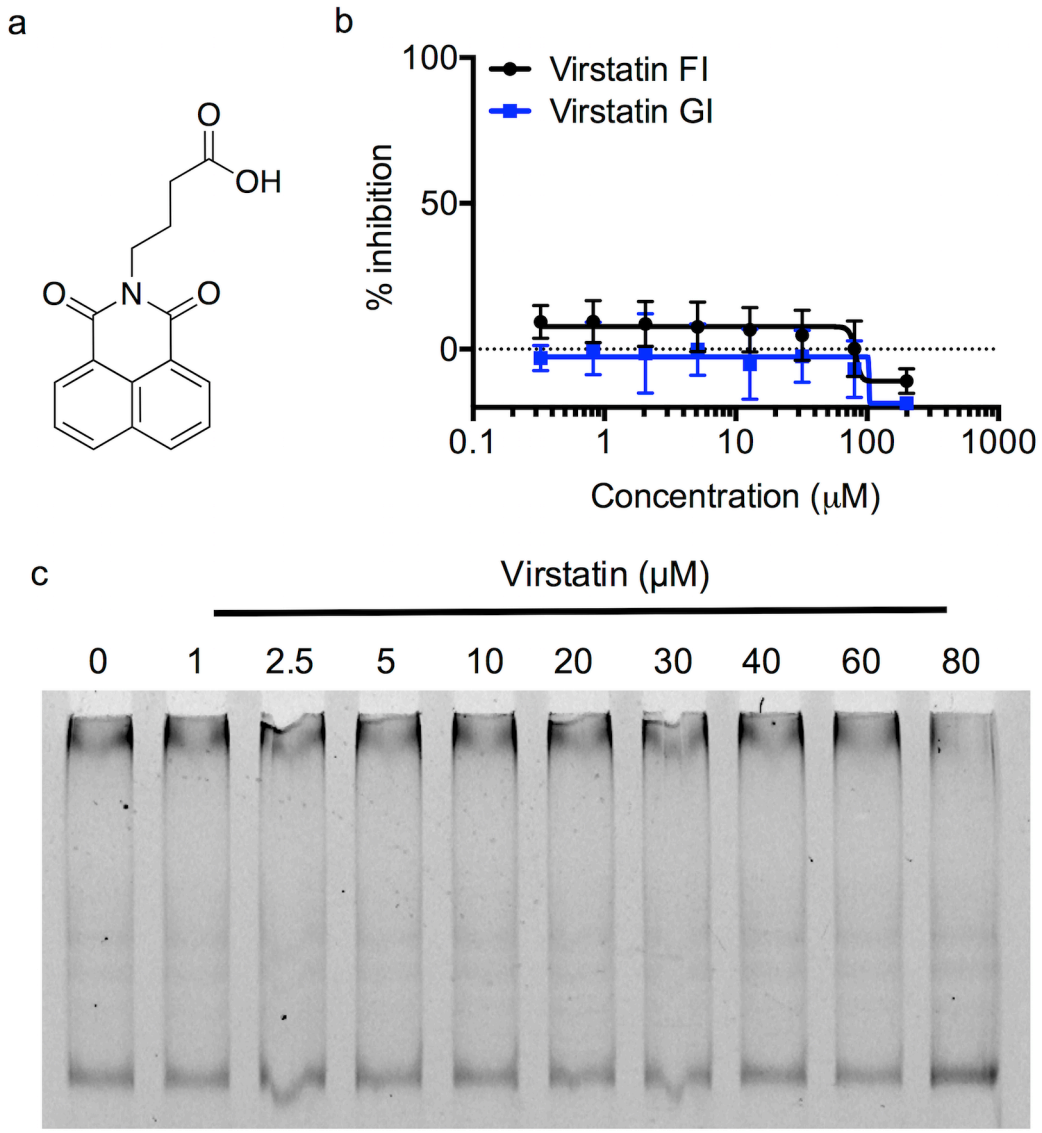

Supplemental Figure 5. The impact of virstatin on DosR DNA-binding and DosRST signaling in Mtb. (a) Chemical structure of virstatin. (b) Dose-response curve of virstatin shows no effect on inhibition of Mtb DosR-driven GFP fluorescence. (c) DosR protein at 2 μM was treated with 9 point dose response of virstatin from 1 μM to 80 μM. The reactions were analyzed on native PAGE gel. The experiment was repeated at least twice with similar results.

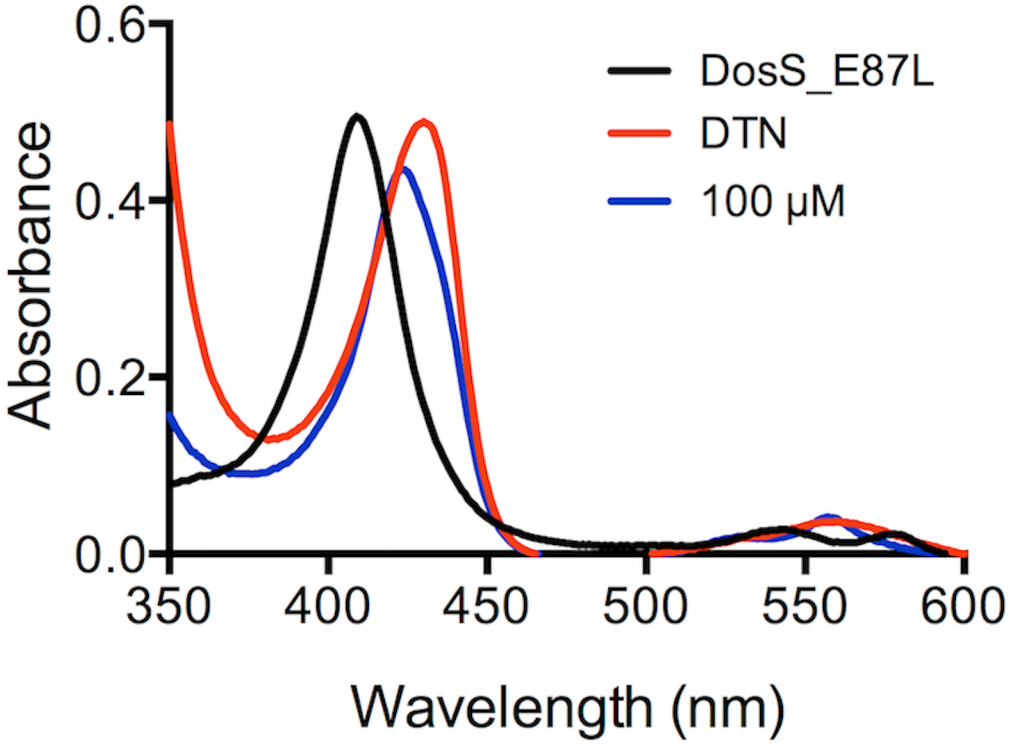

Supplemental Figure 6. Investigating the interaction between HC106A and DosS heme. DosS E87L protein was treated with 100 μM HC106A after being reduced with DTN. The UV-visible spectra were recorded after each treatment, and showed no change on the overall spectrum compared to WT protein. The experiment was repeated at least twice with similar results.

A

HC103A (μM)

HC102A (μM)	50	20	8	3.2	1.28	0.51	0.21	0.08
50	0.14	0.28	0.43	0.34	0.38	0.44	0.5	0.49
20	0.19	0.39	0.32	0.33	0.41	0.58	0.75	0.82
8	0.21	0.45	0.38	0.47	0.62	0.91	1.13	1.33
3.2	0.3	0.55	0.61	0.71	0.99	1.18	1.49	1.89
1.28	0.44	0.72	0.9	1.14	1.22	1.55	1.87	2.99
0.51	0.43	0.85	1.11	1.24	1.28	1.35	1.86	4.2
0.21	0.43	0.94	1.19	1.37	1.4	1.59	3.61	13.8
0.08	0.43	0.94	1.2	1.32	1.27	1.18	1.51	5.84

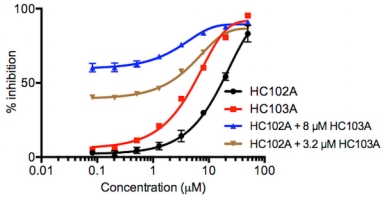

HC104A (μM)

HC102A (μM)	50	20	8	3.2	1.28	0.51	0.21	0.08
50	0.33	0.53	0.85	0.77	0.76	0.77	0.75	0.74
20	0.33	0.73	1.06	1.12	1.19	1.19	1.13	1.04
8	0.31	0.89	1.36	1.64	1.76	1.75	1.69	1.57
3.2	0.28	1.06	1.58	1.91	2.13	2.06	2.18	2.32
1.28	0.28	1.11	1.65	2.05	2.3	2.67	3.05	7.27
0.51	0.27	1.11	1.66	1.95	2.27	2.6	3.81	46.9
0.21	0.29	1.12	1.68	2.06	2.26	3.21	5.22	5.7
0.08	0.27	1.09	1.61	1.9	2.17	2.28	3.1	9.43

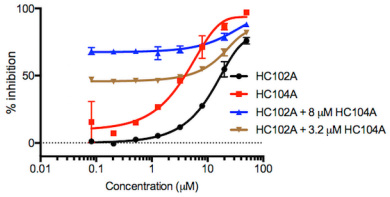

HC106A (μM)

HC102A (μM)	50	20	8	3.2	1.28	0.51	0.21	0.08
50	0.82	0.37	0.33	0.31	0.33	0.39	0.44	0.5
20	0.85	0.4	0.43	0.46	0.49	0.58	0.63	0.7
8	0.64	0.42	0.8	0.9	0.81	0.82	0.99	1.05
3.2	0.71	0.42	1.36	1.29	1.18	1.62	1.12	1.27
1.28	0.72	0.42	1.64	1.69	1.4	1.3	1.3	1.47
0.51	0.72	0.44	1.74	1.59	1.47	1.21	1.24	1.32
0.21	0.7	0.41	1.78	1.87	1.52	1.35	1.49	1.72
0.08	0.71	0.43	1.66	1.67	1.37	1.25	1.14	0.91

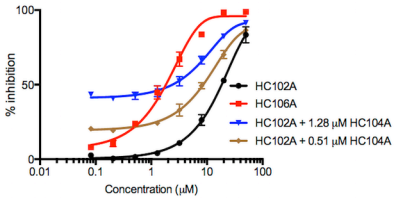

HC104A (μM)

HC103A (μM)	50	20	8	3.2	1.28	0.51	0.21	0.08
50	0.67	0.29	0.35	0.44	0.48	0.64	0.56	0.55
20	0.52	0.5	0.79	0.96	1.11	1.3	1.17	1.22
8	0.45	0.76	1.03	1.22	1.38	1.56	1.54	1.47
3.2	0.42	1.01	1.23	1.35	1.49	1.87	1.92	1.72
1.28	0.39	1.07	1.34	1.42	1.52	1.76	1.87	1.91
0.51	0.4	1.13	1.43	1.47	1.5	1.53	0.95	2.02
0.21	0.39	1.16	1.43	0.94	1.41	1.41	1.78	3.2
0.08	0.16	1.18	1.44	1.47	1.44	1.24	1.26	3.37

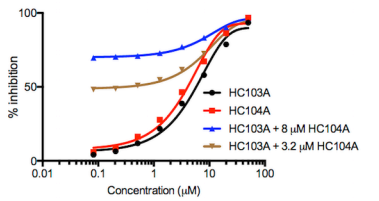

HC106A (μM)

HC103A (μM)	50	20	8	3.2	1.28	0.51	0.21	0.08
50	1.23	0.54	0.3	0.22	0.2	0.27	0.35	0.51
20	1.04	0.44	0.2	0.25	0.39	0.74	0.81	1.03
8	0.96	0.43	0.3	0.72	0.65	0.79	1	1.19
3.2	0.78	0.41	0.6	0.89	0.96	1	1.13	1.24
1.28	0.87	0.44	1.1	1.56	1.38	1.37	1.29	1.3
0.51	0.82	0.48	1.5	1.95	1.64	1.61	1.59	1.44
0.21	0.89	0.48	1.9	2.16	1.93	1.73	1.99	2.5
0.08	0.82	0.46	2.2	2.08	2.29	1.79	2.1	2.74

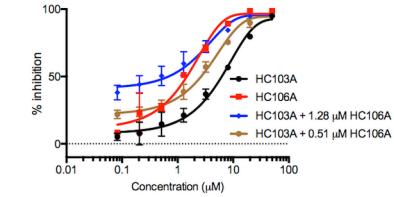

HC106A (μM)

HC104A (μM)	50	20	8	3.2	1.28	0.51	0.21	0.08
50	1.79	1.05	0.65	0.51	0.45	0.44	0.86	0.55
20	1.35	0.64	0.52	0.65	0.83	0.99	1.11	1.16
8	1.05	0.53	0.78	0.97	1.11	1.38	1.52	1.55
3.2	0.84	0.48	0.96	1.11	1.22	1.45	1.58	1.62
1.28	0.77	0.51	1.29	1.68	1.42	1.73	1.67	1.64
0.51	0.88	0.52	1.44	1.45	1.47	1.64	1.68	1.46
0.21	0.8	0.4	1.72	1.62	0.94	1.3	1.76	1.51
0.08	0.79	0.44	1.69	1.59	1.43	1.5	1.46	1.35

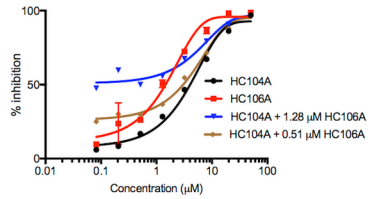

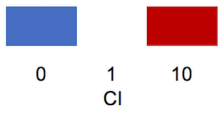

Supplemental Figure 7. Checkerboard assays examining paired interactions of DosRST inhibitors. CDC1551 (hspX'::GFP) was treated with different combination of two compounds from 50 μM to 0.08 μM. GFP fluorescence was measured and used to calculate percentage inhibition. The data were analyzed in the CompuSyn software to determine the combination index (CI) for the panel of each drug combination, including (a) artemisinin and HC104A; (b) HC102A and HC103A; (c) HC102A and HC104A; (d) HC102A and HC106A; (e) HC103A and HC104A; (f) HC103A and HC106A; (g) HC104A and HC106A. Selected dose response curves are presented to illustrate synergistic interactions. The experiment was repeated twice with similar results.

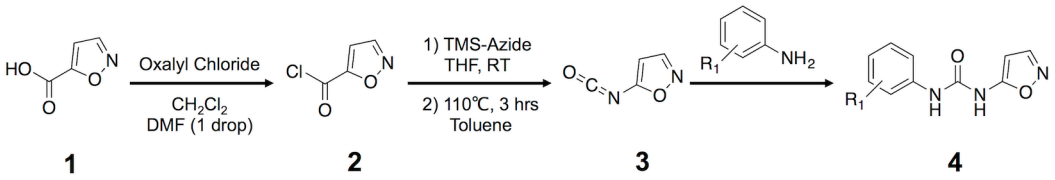

Supplemental Figure 8. Synthetic scheme for the HC106 analogs.

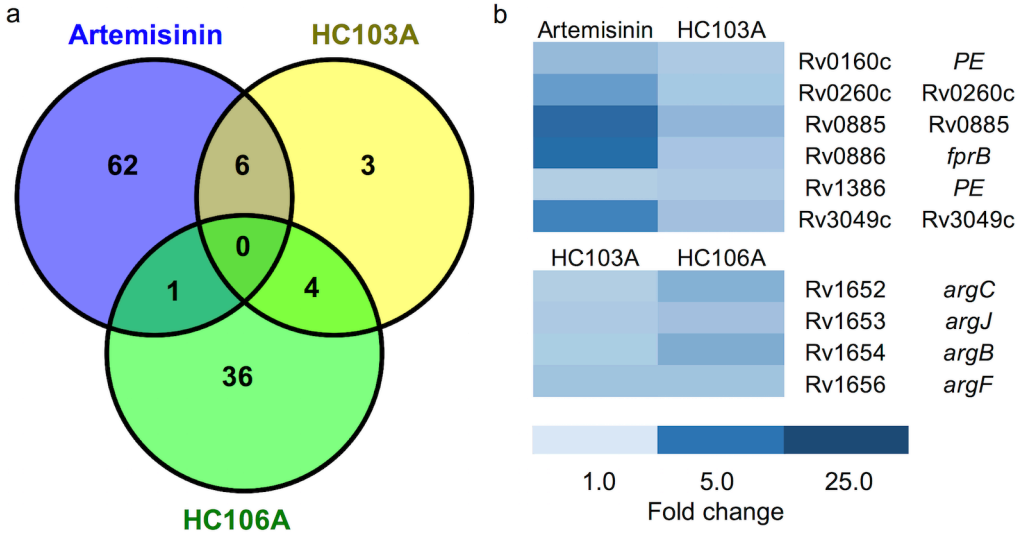

Supplemental Figure 9. Comparison between artemisinin, HC103 and HC106 for interactions. (a) Venn diagram for the downregulated genes (>2-fold; q< 0.05) of CDC1551 (ΔdosR) treated with artemisinin, HC103A, or HC106A. (b) Overlap exists between artemisinin and HC103A or HC103A and HC106A differentially expressed genes (downregulated >2X, q<0.05). The heatmaps represent the commonly downregulated genes between the two compounds.